nature portfolio

Peer Review File

Single-cell Encoded Gene Silencing for High-throughput Combinatorial siRNA Screening

Corresponding Author: Professor Peng Shi

This file contains all reviewer reports in order by version, followed by all author rebuttals in order by version.

Version 0:

Reviewer comments:

Reviewer #1

(Remarks to the Author)
This is an interesting study on the development of a high throughput screening method for combinatorial siRNA based on Au and iron oxide assembled beads. The design is neat. The authors clearly showed the preparation of the knock beads by hierarchical assembly. The feasibility and the potential applications of the method are demonstrated. The following are some suggestions that may further improve the clarity and enhance the accuracy of the study.
1. The manuscript does not seem to explain how siRNA is released from the complex after the application of infrared induces cell membrane perforation. Given that siRNA is initially bound to nanoparticles through electrostatic interactions, how does it detach and effectively enter the cells post-perforation? Moreover, is there a variance in the difficulty of detachment and the efficiency of cellular entry among different siRNAs?
2. The method relies on the knock-beads remaining on the cell membrane for decoding and analysis. Will the beads move from one cell to another cell through direct interaction or cell endocytosis and exocytosis?
3. The further improvement of this screening method's efficiency is constrained because it is hard to incorporate additional fluorophores without disrupting each other for fluorescence encoding. Thus, it’s challenging to simultaneously screen hundreds or thousands of siRNA combinations as proposed in the manuscript, due to these inherent limitations in fluorophore compatibility and availability.
4. In the process where gold nanorods are cross-linked to iron oxide particles using glutaraldehyde crosslinking, why does the zeta potential increase after the amine groups transformed to imine groups?
5. The number of beads interacting with cells is following a Gaussian-like distribution ranging from 1 to 6. How do the authors determine the proper (numbers) dose of the knock beads? Will the dose affect the combinatorial screening of siRNA cocktails?
6. In Figure 4a, the intracellular delivery of siRNA shows obvious cell differences. Some of the siRNA are only distributed on the cell membrane. How to identify these cells? The method to identify and segment the cells may be further explained.
7. Other minor points:
1) The confocal microscopic images of Figure 2c,d were obtained after the assembly procedure. The figure caption description as “before connecting them to Au nanorods or Fe3O4 beads” is confusing.
2) The authors concluded that siRNA-cy5 was delivered into cells in contact with only KB1-Cy5 (Figure 4a), which is different from the quantitative result of Figure 4e. The authors should be more exact in describing the result.
3) It would be beneficial for the manuscript to undergo a thorough review for consistent terminology usage, such as "Cy5" or "cy5".

Reviewer #2

(Remarks to the Author)
The author presented a novel technology where nano-/micro composite carrier material is utilized for high throughput combinatorial siRNA screening. This interesting new technology could greatly boost the efficiency of the identification of effective siRNA combinations for gene therapies. However, authors need to address the following issues prior to publication:

1. Line 190 typo "safty".

2. The cell viability was measured right after irradiation. What about the chronic toxicity long term? Large, heavy and cationic particle plus photo energy absorption could cause significant cytotoxicity if incubated with cells overnight.

3. Figure 2f,g missing data for the siRNA loaded particles.

4. what does the different colors in figure 4d mean?

5. Why not used siRNA-loaded and fluorophore-tagged nanoparticles that can enter cytoplasm for this application so that nanoparticles can reliably label the cells from within the cytoplasm without needing a magnetic field for the tight interface.

6. Line 288, what was used as the negative control, beads without siRNA or with scrambled sequence siRNA?

7. Line 300, Why the maximum siRNA is 5 not 6? And how come the there were only 54 combinations presented in figure 5f?

8. Should Figure 5e means the number of TYPES of knock beads on a single cell instead of number of knock beads on a single cell as Figure 5f's results were derived from the combination between 6 different types of siRNA/knock bead not total number of siRNA/knock bead on a single cell?

9. What do the black dots in figure 6 a,b,d,e mean? Each dot means one cell? The description of the experimental methods presented in figure 6 in unclear and unfound in materials and method section.

Reviewer #3

(Remarks to the Author)
Guo et al. proposed a novel combinatorial siRNA screening method suitable for screening siRNA-based cocktail therapeutics in a massively multiplexed, quantitative, and systematic manner. They utilized assembled nano-/micro composite carriers responsive to near-infrared light and magnetic fields to enable photoporation-induced cellular transfection of RNAs with single-cell resolution. Their innovative approach offers versatile application possibilities. Nonetheless, further validation is necessary to confirm the effectiveness of the proposed new technology.

1. Given that NIR induces a rise in local temperature around the Knock-beads, it is likely that the heightened concentration of Knock-beads affects cell viability when exposed to NIR, potentially causing thermal damage. Please assess the impact of thermal damage on cell viability in the presence of NIR.

2. In Figure 3d, it is evident that as NIR-irradiation times increase, cell viability decreases. Likewise, if there are numerous Knock-beads surrounding the cell, could this influence cell survival rates compared to fewer Knock-beads due to the cytotoxicity of magnetic nanoparticle?

3. Figures 3e-g demonstrate the binding of siRNAs to Knock-beads. Could you provide an estimation of the binding capacity and affinity of Knock-beads for siRNAs? Additionally, is there any impact of siRNA sequence variation on the binding affinity of Knock-beads for siRNAs? Furthermore, when NIR is applied, does it enhance the dissociation of siRNAs from Knock-beads, or does dissociation occur naturally as an on-off effect? Considering the potential dissociation of siRNAs from Knock-beads under culture conditions, there's a possibility of cross-contamination of siRNAs between Knock-beads. Could you elaborate on the likelihood of such cross-contamination?

4. This screening must be conducted in the presence of a magnetic field. Prior studies have indicated that exposure to a magnetic field can lead to changes in gene expression, particularly in the expression of heat shock proteins (Bioelectromagnetics. 2014;35(6):406-13, PMID: 24839179). Could you offer insights into how exposure to a magnetic field might affect this screening system?

5. Figures 4i and j depict the specific knockdown of actin and tubulin by the respective Knock-beads. I think that there may be a mislabeling in the figure legend for Figure 4i. The top-right panel should correspond to KB-A because the Knock-beads are red, while the bottom-left panel should represent KB-T because the Knock-beads are yellow. Moreover, despite the demonstration of the general knockdown effect of each Knock-bead in Figure 4j, it appears that the expression of tubulin is reduced even in the Knock-bead intended for actin (top-right and bottom-left panels in Figure 4i). Could you please clarify the specific knockdown effect of the Knock-beads?

6. In the proof of concept experiments, the knock-down efficiency of 6 siRNA needs to be evaluated for each target gene of siRNAs.

7. When employing color encoding through rainbow labeling, how many genes can be targeted simultaneously using Knock-beads? Please elaborate on this aspect in the discussion section.

8. In figures 6a and b, apoptosis induction and proliferation inhibition increase with the number of knockdown genes. There is a possibility that this effect is due to non-specific factors such as increased thermal damage resulting from enhanced

binding of Knock-beads to cells, rather than specific gene knockdown effects of siRNAs. Please present experimental evidence demonstrating that this effect is not merely a non-specific consequence of an increased number of siRNAs or Knock-beads.

9. In figures 6d and e, the effects of single-path-2 or single-path-3 may vary depending on the targeted pathways (apoptosis or proliferation). Please compare the effects of single-path-2 or single-path-3 from the apoptosis pathway, proliferation pathway, and their combination on the apoptosis and proliferation.

10. In the discussion, the authors propose the possibility of expanding the siRNA screening throughput to encompass more than 60 genes. It would be valuable to provide experimental evidence showing that this approach can be implemented at the single-cell level using an increased number of Knock-beads. It is suggested that the distribution of the number of Knock-beads on individual cells, as illustrated in Figure 5e, should be demonstrated for at least 20 types of Knock-beads. Additionally, could there be resolution issues when observing a large number of beads, each with different labels, under a microscope? Please elaborate on the resolution issues encountered when using a large number of Knock-beads.

11. As stated in the method (Lines 507–508), the TUNEL Apoptosis Assay was conducted after 20 hours of photoporations. This timeframe could be beneficial for identifying genes associated with short-term cell death. However, if employing combinatorial siRNA screening to unveil genes involved in long-term cell death, it's pertinent to consider whether spectrum-coded Knock-beads can sustain the stability of fluorophores and, if so, for how long.

Version 1:

Reviewer comments:

Reviewer #1

(Remarks to the Author)
The authors have addressed all the comments. The quality of the manuscript has been improved. Thus, I would like to recommend the acceptance of the work.

Reviewer #2

(Remarks to the Author)
The authors have adequately addressed all my comments and provided new insights that further elucidate the merits of their studies. This manuscript is in a good shape for publication.

Reviewer #3

(Remarks to the Author)
I would like to thank the authors for their efforts. All concerns raised by this reviewer are resolved.

REVIEWER COMMENTS

Reviewer #1 (Remarks to the Author): This is an interesting study on the development of a high throughput screening method for combinatorial siRNA based on Au and iron oxide assembled beads. The design is neat. The authors clearly showed the preparation of the knock beads by hierarchical assembly. The feasibility and the potential applications of the method are demonstrated. The following are some suggestions that may further improve the clarity and enhance the accuracy of the study.

We thank the reviewer for the generally positive comments.

1. The manuscript does not seem to explain how siRNA is released from the complex after the application of infrared induces cell membrane perforation. Given that siRNA is initially bound to nanoparticles through electrostatic interactions, how does it detach and effectively enter the cells post-perforation? Moreover, is there a variance in the difficulty of detachment and the efficiency of cellular entry among different siRNAs?

Regarding the mechanism of siRNA release and cellular entry, we believe that the Poly dimethyl diallyl ammonium chloride (PDDA) layer coating on the surface of the Fe_3O_4-Au beads plays a critical role via van der Waals interactions (*Liu 2015, Kaur 2018, He 2023, Luo 2015*). The PDDA layer was used to electrostatically capture siRNAs. At nanometer scale, the van der Waals adhesion between PDDA and Fe_3O_4-Au bead is increasingly affected by thermal fluctuations (*Carrillo 2012*). Pinon *et al*. demonstrated that a temperature increase of just 23K can lead to a substantial decrease in van der Waals adhesion force from 106 nN to 28 nN (*Pinon 2016*). In our system, the temperature of the Knock-beads was changed by gold nanorod-induced surface plasmon resonance (*Amendola 2017, You 2021*). The local temperature increase in each Knock-bead disrupts the van der Waals interactions, causing the PDDA-siRNA to detach from the Knock-beads (**Figure R1.1**). As shown in **Figure R1.1**, we used ~8×10^5 Knock-beads to absorb 20 pmol siRNA-cy5 in the solution through electrostatic interaction. The siRNA loaded Knock-beads were pulled down to the bottom of the reaction tube by an external magnet. Upon NIR irradiation for 2, 4, 6, 8 seconds, the siRNAs were released to the solution by 53.5%, 63.4%, 80.3% and 87.0% of the total load, as reflected by the increase of the fluorescence of the supernatant solution.

Meanwhile, as the result of the photoporation of the cells in contact with Knock-beads, the local temperature rise enhances the mobility of lipid molecules and causes a local phase transition the lipid bilayer. The positively charged PDDA-RNA interacts with negative charged cell membrane by electrostatic interaction, facilitating its intracellular translocation. After entering a cell, the increase of acidity weaken the electrostatic interaction between RNA and PDDA (*Xu 2020*). This part of discussion has been included in the revised manuscript: "Result" section **(Page 10, line 259 to line 266)** and "Discussion" section (**Page 19, line 473 to Page 20, line 482**)

For the release of different siRNAs, we tested 8 different types of siRNAs (cy5-labeled), which were designed with different sequences targeting actin, tubulin, Bcl-2, survivin, Mcl-1, c-Myc, cyclin D1 and PLK-1, respectively. The result showed that no significant change of releasing efficiency (from Knock-beads) was observed among these siRNAs (**Figure R1.2**). Following the same photoporation procedure, similar cellular entry efficiencies were also observed among these siRNAs, as shown by our flow cytometry analysis of the treated cells (**Figure R1.3**). This part of discussion has been included in the revised manuscript, "Result" section (**Page 10, line 264 to line 266**).

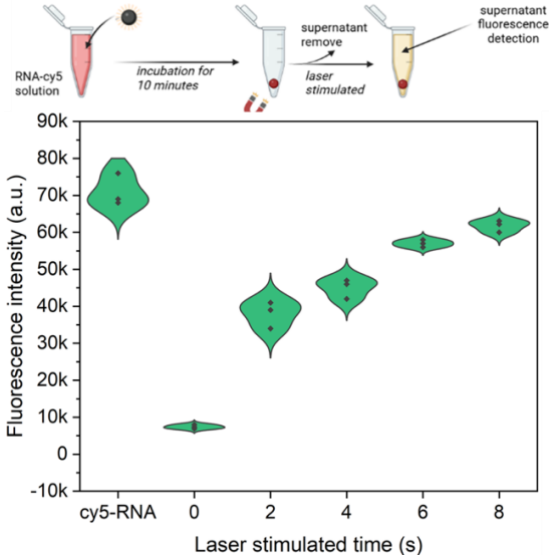

Figure R1.1. Violin plot showing the characterization of siRNA release from the Knock-beads upon NIR irradiation. Fluorescence intensity of the supernatant solution was measured to reflect the RNA capture by the Knock-beads or RNA release from the Knock-beads upon NIR irritation of different duration from 2 to 8 seconds. "0" indicates the depletion of fluorescence by ~8×10^5 Knock-beads to absorb 20 pmol siRNA-cy5 in the solution through electrostatic interaction. The siRNA loaded Knock-beads were pulled down to the bottom of the reaction tube by an external magnet. Upon NIR irradiation for 2, 4, 6, 8 seconds, the siRNAs were released to the solution by 53.5%, 63.4%, 80.3% and 87.0% of the total load, as reflected by the recovery of the fluorescence of the supernatant solution. N = 3, the dots in the violin plots indicate the data points for individual experiments. This figure is included in the revised supporting information as **Supplementary Figure S4**.

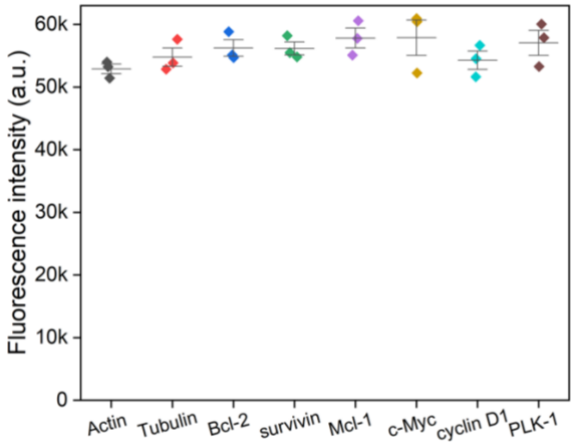

Figure R1.2. Sequence-specific variation of siRNA release from the Knock-beads. Fluorescence intensity of supernatant solution was measured after siRNAs (cy5 labeled) release from the Knock-beads upon 6 second laser irradiation. 8 different types of siRNAs (cy5-labeled) were tested. They were designed with different sequences targeting actin, tubulin, Bcl-2, survivin, Mcl-1, c-Myc, cyclin D1 and PLK-1, respectively. No significant change of releasing efficiency was observed among these siRNAs, N = 3, statistics by student T-test. This figure is included in the supporting information as **Supplementary Figure S5**.

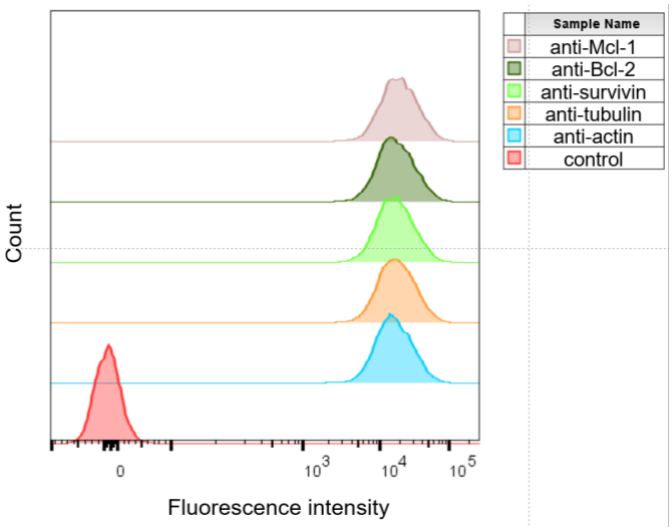

Figure R1.3. Sequence-specific variation of siRNA intracellular translocation upon photoporation. This figure shows the intracellular translocation of 5 different siRNAs 4 hours after photoporation treatment. The siRNA was loaded on the Knock-beads and then applied the cells followed by a photoporation treatment. After 4 hours, the cells were analyzed using flow cytometry to assess the uptake of the fluorescence labeled siRNA. The negative control group refers to a sample that did not receive any photoporation. This figure was included in the supporting information as **Supplementary Figure S6**.

References:

- Liu X, *et al.* Understanding the Effect of Different Polymeric Surfactants on Enhancing the Silicon/Reduced Graphene Oxide Anode Performance. *The Journal of Physical Chemistry C* 2015, **119**(11)**:** 5848-5854.
- Kaur P, *et al.* Supramolecular modification of Carbon Nanofibers with Poly(diallyl dimethylammonium) chloride and Triton X-100 for electrochemical application. *International Journal of Hydrogen Energy* 2018, **43**(13)**:** 6575-6585.
- He X, *et al.* Bimodal Antimicrobial Surfaces of Phytic Acid-Prussian Blue Nanoparticles-Cationic Polymer Networks. *Adv Sci (Weinh)* 2023, **10**(16)**:** e2300354.
- Luo D, *et al.* Interparticle Forces Underlying Nanoparticle Self-Assemblies. *Small* 2015, **11**(45)**:** 5984-6008.
- Carrillo J-MY, *et al.* Dynamics of nanoparticle adhesion. *The Journal of Chemical Physics* 2012, **137**(21).
- Pinon AV, *et al.* Thermal effects on van der Waals adhesive forces. *Physical Review B* 2016, **93**(3).
- Amendola V, *et al.* Surface plasmon resonance in gold nanoparticles: a review. *J Phys Condens Matter* 2017, **29**(20)**:** 203002.
- You M, *et al.* Quantifying and Adjusting Plasmon-Driven Nano-Localized Temperature Field around Gold Nanorods for Nucleic Acids Amplification. *Small Methods* 2021, **5**(5)**:** e2001254.
- Xu X, *et al.* Effective Delivery of the CRISPR/Cas9 System Enabled by Functionalized Mesoporous Silica Nanoparticles for GFP-Tagged Paxillin Knock-In. *Advanced Therapeutics* 2020, **4**(1).

2. The method relies on the knock-beads remaining on the cell membrane for decoding and analysis. Will the beads move from one cell to another cell through direct interaction or cell endocytosis and exocytosis?

We concur with the reviewer that the mobility of the Knock-beads from one cell to another could potentially cause diffused error for decoding and analysis. Therefore, it is very important to make sure that the Knock-beads remain fixed on the cells during the analytical process. After application, the Knock-beads were firstly bound to the cell membrane through electrostatic interaction. At the live culture stage, the Knock-beads were further immobilized on the contacting cells using a neodymium magnet (10 kilo-Gauss), which was sufficiently large to prevent the beads from moving around. At the decoding and analysis stage, the cells and the Knock-beads were fixed used polyformaldehyde, where the remaining -NH_2 group on the Knock-beads and cell cytoskeleton was crosslinked. Throughout the processes, the neodymium magnet was kept attached to the bottom of the culture dish to provide sustained restriction of the Knock-beads.

Regarding the cell endocytosis and exocytosis concern raised by the reviewer, the microscale Knock-beads are unlikely to be internalized by the cells via endocytosis due to the physical size (~4.4 μm) (*Kohane 2007*). *Gratton et al*. has reported that micro-particles larger than 3 μm almost do not enter cells (*Gratton 2008*).

Taken together, the combination of magnetic fixation, chemical cross-linking, and size constraints ensures that the Knock-beads remain stably associated with the contacting cells throughout culturing, decoding and analysis processes, which is a critical aspect of the experimental design to allow single-cell-based encoding/decoding of the molecular information by the Knock-beads. This part of discussion has been added to the manuscript, "Discussion" section **(Page 20, line 488 to line 499).**

References:

- Kohane DS. Microparticles and nanoparticles for drug delivery. *Biotechnol Bioeng* 2007, **96**(2)**:** 203-209.
- Gratton SE*, et al.* The effect of particle design on cellular internalization pathways. *Proc Natl Acad Sci U S A* 2008, **105**(33)**:** 11613-11618.

3. The further improvement of this screening method's efficiency is constrained because it is hard to incorporate additional fluorophores without disrupting each other for fluorescence encoding. Thus, it's challenging to simultaneously screen hundreds or thousands of siRNA combinations as proposed in the manuscript, due to these inherent limitations in fluorophore compatibility and availability.

As pointed out by the reviewer, the translational potential of a high-throughput technology relies heavily on its extendibility for largescale screens, which appears to be constrained by the availability of fluorophores for simultaneous imaging.

However, the development encoding strategies could overcome this challenge by increasing the screening capacity exponentially. For example, *Shi et al.* have shown that they can use 10 different fluorophores to encode over a thousand (2^{10} - 1) *E. coli* variants using a machine learning technique (*Shi 2020*). Extended from our work in the first submission, in this revision, we further demonstrated the use of a 5-channel system for multiplexed encoding of more than 30 Knock-beads variants.

Specifically, we used a combinatory fluorescence labeling of the Knock-beads to substantially increase the multiplexing throughput by using 5 fluorescent channels. Each Knock-bead was made with a programmed rainbow fluorescence composed of 5 different fluorophores (quantum dot 547, 572, 604, 641, and Alexa fluor 647). For spectrum digitization, we used "1" to denote the inclusion and "0" to denote the exclusion of a fluorophore and to compose a 5-digit spectral code for each Knock-bead variant. In this way, a 5-channel fluorescent system is expanded to encode 31 Knock-bead variants (2^5 – 1=31, **Table R1.1**), each of which was assigned to a specific siRNA. At analytical microscopy stage, the optical spectrum of the Knock-beads was decoded by using a machine learning algorithm (**Figure R1.4**). By using this system, we were able to demonstrate an expanded screening involving 20 siRNA target genes and tested more than 1300 Knock-combos composed of 1, 2, or 3 siRNAs for combinatorial knocking down (**Figure 7**).

The screening results were summarized in the newly included **Figure 7.** While the apoptosis level varied among different Knock-combos, it was clearly observed multi-pathway knock-down was more effective than just targeting a single-pathway. Such synergic efficacy becomes even more evident for 3 siRNA combinations (**Figure 7a-c**), which is consistent with our observations in the smaller scale screening and emphasizes the importance and unique advantage of our innovation for high-throughput combinatorial siRNA screening. For all the 1315 siRNA Knock-combos, K-means clustering analysis was used to discover two distinct clusters, one of which showed significantly better efficacy for apoptosis induction (**Figure 7d, e, Supplementary Figure S17**). We then derived a relative ratio to show the enrichment of individual siRNA in each cluster (cluster 1, 2), showing the top-6 dominant role of cyclin D1, survivin, HER-2, Hsp 27, Upar and GSK 3a for the apoptosis-pro cluster (cluster 1, **Figure 7f**), which are well-represented in the top-2 apoptosis-pro Knock-combos (**Figure S20**). We then used a network interaction diagram to analyze the synergic efficacy from multiple siRNAs (**Figure 7g**). As a hub gene, HER2 or cyclin D1 showed the most connections to other genes, suggesting the important contributions from siRNAs targeting complementary genes. On the other hand, uPAR gene appeared to be the best silencing partner for many leading siRNA targeting either survivin or HER2. These screening results provides valuable insights to the construction of combinatorial siRNAs therapeutics for anti-tumor purpose.

Furthermore, an extension to a 10-channel system (*Shi 2020*) with binary labelling ("0" or "1") would increase the multiplexing capacity to 1023 genes, which would further render millions of Knock-combos. If a screening is designed to target the combinatory silencing of 2 or 3 genes with siRNA combos, the total possible Knock-combos would be 178,433,024 ($C_{1023}^2 + C_{1023}^3$), which is a number almost inaccessible to any existing methods.

This part of discussion has been added to the manuscript, "Result" section **(Page 17, line 411 to Page19, line 453).**

References:

- Shi H*, et al.* Highly multiplexed spatial mapping of microbial communities. *Nature* 2020, **588**(7839)**:** 676-681.

Table R1.1. Spectrum encoding of different Knock-beads using a 5-channel fluorescent system (quantum dot 547, 572, 604, 641, and Alexa fluor 647). The shaded region indicates the extra code not used in the expanded large-scale screening. This table is included in the supporting information as **Supplementary Table S5**.

Knock-bead index	Quantum dot-547	Quantum dot-572	Quantum dot-604	Quantum dot-641	Alexa-647	Code
1	100%	0	0	0	0	10000
2	0	100%	0	0	0	01000
3	0	0	100%	0	0	00100
4	0	0	0	100%	0	00010
5	0	0	0	0	100%	00001
6	100%	100%	0	0	0	11000
7	100%	0	100%	0	0	10100
8	100%	0	0	100%	0	10010
9	100%	0	0	0	100%	10001
10	0	100%	100%	0	0	01100
11	0	100%	0	100%	0	01010
12	0	100%	0	0	100%	01001
13	0	0	100%	100%	0	00110
14	0	0	100%	0	100%	00101
15	0	0	0	100%	100%	00011
16	100%	100%	100%	0	0	11100
17	100%	100%	0	100%	0	11010
18	0	100%	100%	100%	0	01110
19	0	0	100%	100%	100%	00111
20	100%	0	100%	100%	100%	10111
21	100%	100%	100%	100%	100%	11111
22	100%	100%	0	0	100%	11001
23	100%	0	100%	100%	0	10110
24	100%	0	100%	0	100%	10101
25	100%	0	0	100%	100%	10011
26	0	100%	100%	0	100%	01101
27	0	100%	0	100%	100%	01011
28	100%	100%	100%	100%	0	11110
29	100%	100%	100%	0	100%	11101
30	100%	100%	0	100%	100%	11011
31	0	100%	100%	100%	100%	01111

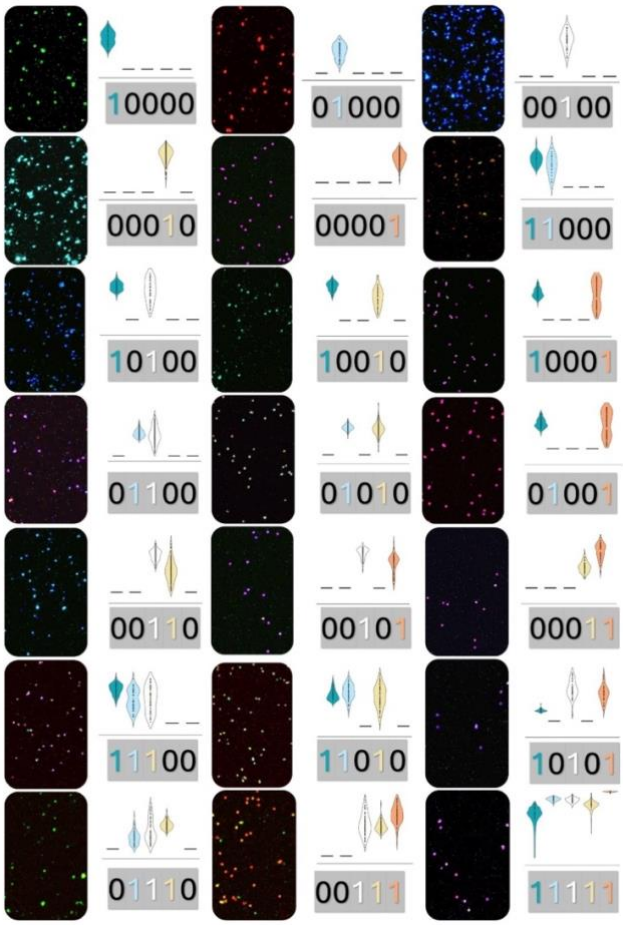

Figure R1.4. Representative images showing the encoded fluorescence signal of 21 Knock-bead variants. A combinatory fluorescence labeling of the Knock-beads was used to substantially increase the multiplexing throughput by using 5 fluorescent channels. Each Knock-bead was made with a programmed rainbow fluorescence composed of 5 different fluorophores (quantum dot 547, 572, 604, 641, and Alexa fluor 647). For spectrum digitization, we used "1" to denote the inclusion and "0" to denote the exclusion of a fluorophore and to compose a 5-digit spectral code for each Knock-bead variant. This figure is included in the supporting information as **Supplementary Figure S15**.

4. In the process where gold nanorods are cross-linked to iron oxide particles using glutaraldehyde crosslinking, why does the zeta potential increase after the amine groups transformed to imine groups?

The overall increase in zeta potential after this crosslinking step is due to the changes in the surface charge composition of the final micro/nano assembly. Initially, the iron oxide (Fe_3O_4) particles were positively charged due to the existence of primary amine ($-NH_2$) groups on their surface. When the glutaraldehyde crosslinking occurs, these amine groups are transformed into imine (-N=CH-) groups, reducing the overall positive charge on the Fe_3O_4 bead surface (zeta potential reduces from + 6.34 mV to +3.99 mV). Next, the linkage of the gold nanorods to the Fe_3O_4 particles introduces additional primary amine ($-NH_2$) groups, which overwhelm the effects of the glutaraldehyde crosslinking and caused the increase in zeta potential to +18.16 mV as observed in **Figure R1.5**. This part of discussion has been added to the manuscript "Result" section (Page 7, line 206) and supporting information, **Supplementary Note 1 (**Page 2, line 31 to line 39**).**

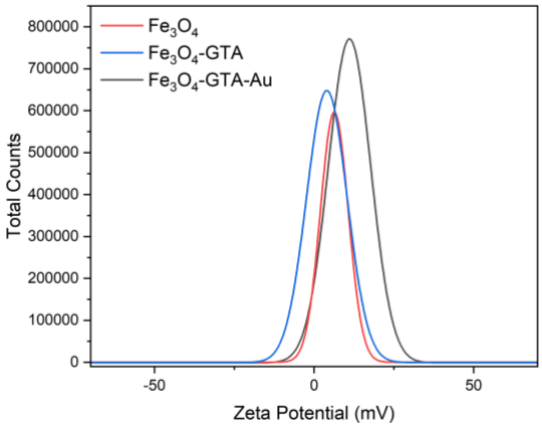

Figure R1.5. Change of zeta potential over the functional preparation of the Knock-beads. the iron oxide (Fe_3O_4) particles were positively charged due to the existence of primary amine ($-NH_2$) groups on their surface. When the glutaraldehyde (GTA) crosslinking occurs, these amine groups are transformed into imine (-N=CH-) groups, reducing the overall positive charge on the Fe_3O_4 bead surface (zeta potential reduces from + 6.34 mV to +3.99 mV). Next, the linkage of the gold nanorods to the Fe_3O_4 particles introduces additional primary amine ($-NH_2$) groups, which overwhelm the effects of the glutaraldehyde crosslinking and caused the increase in zeta potential to +18.16 mV. This figure is included in the supporting information as **Supplementary Figure S1**.

5. The number of beads interacting with cells is following a Gaussian-like distribution ranging from 1 to 6. How do the authors determine the proper (numbers) dose of the knock beads? Will the dose affect the combinatorial screening of siRNA cocktails?

Before addressing the effects from the bead number distribution, we would like to clarify one fact: in many drug combination therapies, such as the cocktail anti-viral therapy for HIV/AIDS management, 2 to 3 active components are typically used. As shown in **Table R1.2** (*Li 2022*), among more than 20 antiretroviral cocktails, 18 formulations are made of 2 to 3 components and only 2 formulations consist of 4 components. Recently, *Tieu et al*. developed a CRISPR-Cas9-based platform for combinatorial gene editing on CAR-T cells also focused on pairwise combinations of different signaling regulators (*Tieu 2024*). Therefore, we believe that the most meaningful siRNA cocktail screening should be oriented towards Knock-combos consisting of 2 to 3 siRNAs.

With this consideration, we specifically optimized the system and controlled the dose of Knock-beads to ensure on average ~3 beads per cell, as shown in **Figure 5e**. As pointed out by the reviewer, the number of beads interacting with the cells follows a Gaussian-like distribution, and the center peak of the distribution could be shifted to lower or higher number per cell by controlling the bead-to-cell ratio (**Figure R1.6**). Certainly, the pattern of Knock-bead distribution is crucial for the effectiveness of the combinatorial screening, as it allows for the capture of a diverse range of cell populations that have been randomly exposed to different combinations of siRNAs (Knock-combos). Increasing the bead dose would shift the distribution toward a higher bead number per cell, potentially reducing the population of cells exposed to the desired 2-3 component siRNA cocktails. Conversely, decreasing the bead dose would result in a lower proportion of cells encountering more complex siRNA combinations, which could potentially limit the capability to uncover some effective siRNA combinations. Additionally, over-dosed Knock-beads causes reduced cell viability at the photoporation stage (**Figure R1.7**), which further require an optimization of the bead-to-cell ratio to construct an effective and efficient screening.

This part of discussion has been added to the manuscript "Result" section (Page 14, line 348), and in "Discussion" section (Page 21, line 513 to line 523), as well as in the supporting information, **Supplementary Note 2** (Page 2, line 41 to line 54).

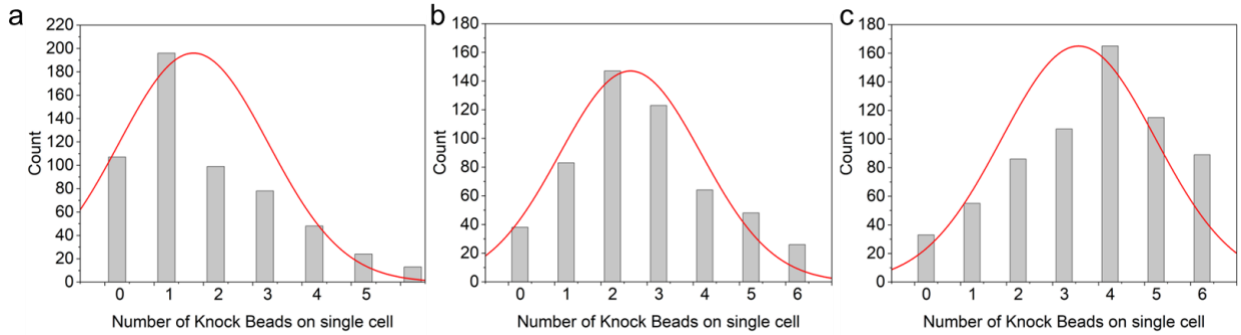

Figure R1.6. Characterization of the Knock-bead distribution per single cell. This figure shows the distribution of the number of Knock-beads per single cell, at different bead-to-cell ratios: 1:1 (a), 2:1 (b), and 4:1 (c). The number of Knock-beads was calculated based on the total number of cells. By controlling the bead-to-cell ratio, we were able to obtain a Gaussian-like distribution of the number of beads interacting with each cell, ranging from 1 to 4 beads per cell. This figure is included in the supporting information as **Supplementary Figure S12**.

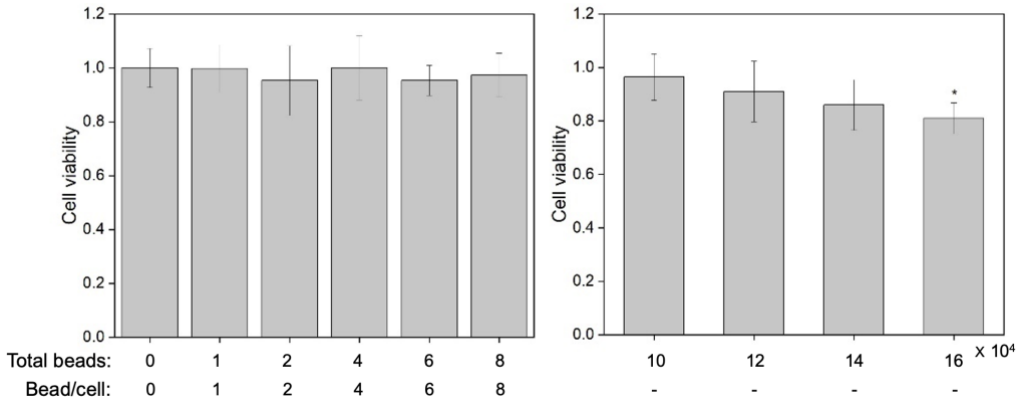

Figure R1.7. Evaluation of cell viability at different Knock-bead to cell ratios. The cell viability was assessed using MTT assay following photoporation treatment at various Knock-bead density. The cells were incubated with Knock-bead at a concentration ranging from 0 to 16 × 10^4. The cell viability was evaluated 24 hours after photoporation. In most screening conditions, the number of Knock-bead per cell would not exceed 8, the photoporation process did not cause any damage in the cells. Only when the Knock-bead density reaches an extremely large level (e.g. 16× 10^4), significant cytotoxicity was observed. This figure is included in the supporting information as **Supplementary Figure S13**.

Table R1.2 List of anti-HIV cocktails and their active components.

Brand name	Ingredients				FDA approve date
Combivir	lamivudine	zidovudine			September 26, 1997
Kaletra	lopinavir	ritonavir			September 15, 2000
Trizivir	abacavir	lamivudine	zidovudine		November 15, 2000
Epzicom	abacavir	lamivudine			August 2, 2004
Triomune	lamivudine	stavudine	nevirapine		not approved
Duovir-N	lamivudine	zidovudine	nevirapine		not approved
Truvada	emtricitabine	tenofovir disoproxil			August 2, 2004
Atripla	emtricitabine	tenofovir disoproxil	efavirenz		July 12, 2006
Complera	emtricitabine	tenofovir disoproxil	rilpivirine		August 10, 2011
Stribild	emtricitabine	tenofovir disoproxil	elvitegravir	cobicistat	August 27, 2012
Triumeq	abacavir	lamivudine	dolutegravir		August 22, 2014
Evotaz	atazanavir	cobicistat			January 29, 2015
Prezcobix	darunavir	cobicistat			January 29, 2015
Dutrebis	lamivudine	raltegravir			February 6, 2015
Genvoya	emtricitabine	tenofovir alafenamide	elvitegravir	cobicistat	November 5, 2015
Odefsey	emtricitabine	tenofovir alafenamide	rilpivirine		March 1, 2016
Descovy	emtricitabine	tenofovir alafenamide			April 4, 2016
Juluca	rilpivirine	dolutegravir			November 21, 2017
Symfi	lamivudine	tenofovir disoproxil	efavirenz		February 5, 2018
Biktarvy	emtricitabine	tenofovir alafenamide	bictegravir		February 7, 2018
Cimduo	lamivudine	tenofovir disoproxil			February 28, 2018
Delstrigo	lamivudine	tenofovir disoproxil	doravirine		August 30, 2018
Dovato	lamivudine	dolutegravir			April 8, 2019
Cabenuva	rilpivirine	cabotegravir			January 21, 2021

References:

- Li G, *et al.* Approved HIV reverse transcriptase inhibitors in the past decade. *Acta Pharmaceutica Sinica B* 2022, **12**(4)**:** 1567-1590.
- Tieu V, *et al.* A versatile CRISPR-Cas13d platform for multiplexed transcriptomic regulation and metabolic engineering in primary human T cells. *Cell* 2024, **187**(5)**:** 1278-1295 e1220.

6. In Figure 4a, the intracellular delivery of siRNA shows obvious cell differences. Some of the siRNA are only distributed on the cell membrane. How to identify these cells? The method to identify and segment the cells may be further explained.

We agree with the reviewer that **Figure 4a** shows some cell-to-cell variations in the siRNA localization after photoporation delivery, and a portion of the siRNA signal distributed primarily on the cell membrane. As this image was taken at the 2-hour point after photoporation, it is likely that the membrane-localized siRNA indicates the intermediate status of the dynamic intracellular translocation of the siRNAs, showing the initial fusion of the PDDA-siRNA with the cell membrane. This observation is consistent with the literature, where similar membrane-associated fluorescence patterns have been reported for using PDDA-coated nanoparticles to deliver Cas9 systems in U2OS cells (*Xu 2020*).

To further clarify this rationale, we have provided additional confocal images taken later time point to monitor the internalization dynamics of the siRNAs (**Figure R1.8**). 5 hours after photoporation, the siRNA signal was predominantly localized within the cytoplasm of the cells, indicating the successful internalization and intracellular delivery of the siRNAs. In the subsequent screening experiments, the cells were all analyzed 24 hours after photoporation, which was a time point allowing for sufficient intracellular translocation of the siRNAs and their associated gene silencing. Relevant discussion has been added to the manuscript, "Result" section (Page 11, line 276 to line 280).

For cell segmentation and Knock-bead identification, more technical details have been included in the "Methods" part of the revised manuscript (**Page 28**, line 662 to line 668).

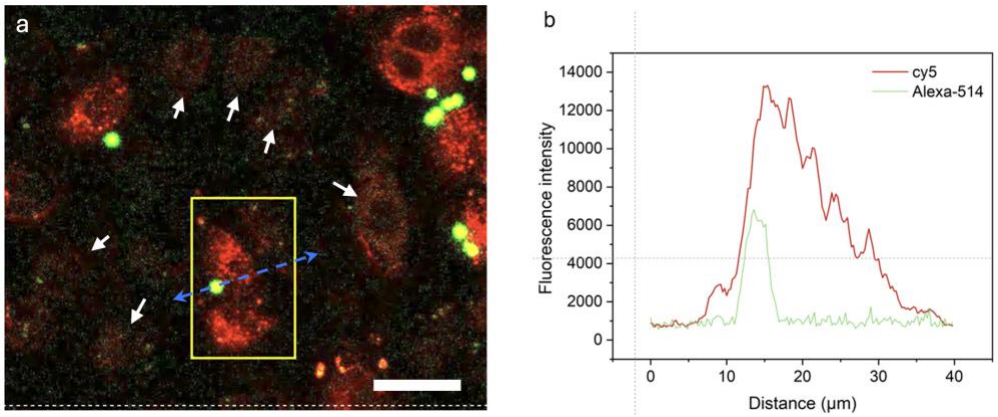

Figure R1.8. Evaluation of siRNA intracellular translocation of siRNA (cy5-Labeled) 5 hours after photoporation. (a) Confocal microscopy image scanning across a horizonal plane sectioning the cells (A549) 5 hours after photoporation treatment. The cells were transfected with cy5-labeled siRNA by using the Knock-bead system. The white arrows indicate the cells without Knock-beads and siRNA delivery. Scale bar, 30 μm. (b) Fluorescence profile along the blue line across the cell in the yellow rectangle in panel (a). This figure is included in the supporting information as **Supplementary Figure S7**.

References:

- Xu X, *et al.* Effective Delivery of the CRISPR/Cas9 System Enabled by Functionalized Mesoporous Silica Nanoparticles for GFP-Tagged Paxillin Knock-In. *Advanced Therapeutics* 2020, **4**(1).

7. Other minor points:

1) The confocal microscopic images of Figure 2c, d were obtained after the assembly procedure. The figure caption description as "before connecting them to Au nanorods or Fe3O4 beads" is confusing.

2) The authors concluded that siRNA-cy5 was delivered into cells in contact with only KB1-cy5 (Figure 4a), which is different from the quantitative result of Figure 4e. The authors should be more exact in describing the result.

3) It would be beneficial for the manuscript to undergo a thorough review for consistent terminology usage, such as "cy5" or "cy5".

We thank the reviewer for his/her careful reading of the manuscript, the text has been thoroughly proofread to improve the readability.

For point (1), we have changed the caption to improve the clarity.
For point (2), we have changed the text for improved clarity.
For point (3), we have unified the use of Cy5/cy5 to cy5 throughout the manuscript.

Reviewer #2 (Remarks to the Author):
The author presented a novel technology where nano-/micro composite carrier material is utilized for high throughput combinatorial siRNA screening. This interesting new technology could greatly boost the efficiency of the identification of effective siRNA combinations for gene therapies. However, authors need to address the following issues prior to publication:
We thank the reviewer for his/her positive comments.

1. *Line 190 typo "safty".*
The typo "safty" is corrected to "safety". We have now carefully proofread the manuscript.

2. The cell viability was measured right after irradiation. What about the chronic toxicity long term? Large, heavy and cationic particle plus photo energy absorption could cause significant cytotoxicity if incubated with cells overnight.
We agree with reviewer that cell viability is very important for a viable screening of therapeutics. To clarify this point, in our first submission, the cell viability (**Figure 3d**) was actually evaluated 24 hours after photoporation, instead of right after NIR irradiation. The temporal window should allow for sufficient cell interaction and response to the physical stimuli induced by the Knock-bead system for evaluating cytotoxicity. In this revision, we have included additional details to clarify the timing of the viability measurements in the manuscript, "Result" section **(Page 9, line 232)** and **Figure 3 caption.**

3. Figure 2f,g missing data for the siRNA loaded particles.
We thank the reviewer for the suggestion. In this revision, we evaluated the zeta potential of the beads when loaded with different amounts of siRNA. As shown in **Figure R2.1**, the Knock-beads zeta potential decreased from 22 ± 0.99 mV to 4.71 ± 1.08 mV, as the amount of loaded siRNA increased from 0 to 80 pmol for a total of 8 x 10^5 beads (equivalent to 0 to 6×10^7 molecules/bead). At even higher siRNA loadings of 160 pmol and 320 pmol (for 8 x 10^5 beads), the zeta potential became negative, measuring -3.33 ± 1.28 mV and -4.4 ± 0.55 mV respectively. In our study, the siRNA load was 20 pmol (equivalent to 9.8×10^6 molecules/bead).

Figure 2e, f has been updated with data for siRNA loaded particles. This part of discussion has been added to the manuscript, "Result" section (Page 9, line 248 to line 254).

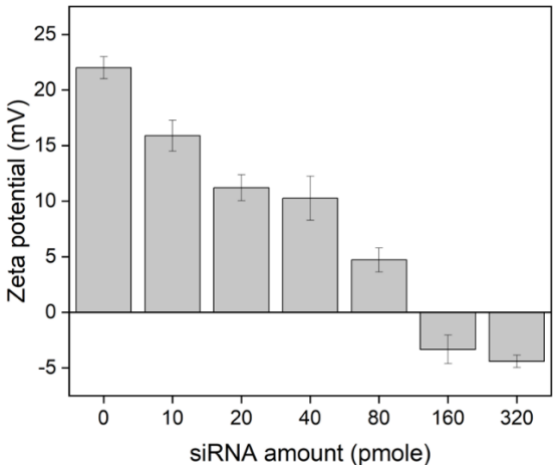

Figure R2.1. Change of Zeta potential for fixed number of Knock-beads (8 x 10^5) with different amount of siRNA input ranging from 0 pmol to 320 pmol. This figure has been added to the supporting information as **Supplementary Figure S2**.

4. *what does the different colors in figure 4d mean?*
In Figure 4d, the colors are used by the image processing algorithm to help discriminate of cell outlines. The color is randomly assigned for improved visualization. We have updated the caption to clarify this point (Page 38, Figure 4 caption).

5. Why not used siRNA-loaded and fluorophore-tagged nanoparticles that can enter cytoplasm for this application so that nanoparticles can reliably label the cells from within the cytoplasm without needing a magnetic field for the tight interface.
The main reason we chose to use the microscale (4.4 μm) Knock-beads in this application is to improve the fluorescence readability to encode/decode the siRNA delivery in individual cells. The microscale Knock-beads are unlikely to be internalized by the cells via endocytosis due to the physical size (*Gratton 2008*). *Gratton et al*. has reported that micro-

particles larger than 3 μm almost do not enter cells (*Pan 2007, Kus 2021*). We believe that leaving the beads outside a cell would cause much less interference to cellular function than the intracellularly delivered ones.

If the nanoparticles are to be intracellularly delivered together with siRNA, their size must be significantly smaller, usually less than 200 nm (*Gratton 2008*). Accordingly, the detection and discrimination of individual nanoparticles within a crowded cellular environment can be challenging by using standard confocal microscopy. The potential cytotoxicity associated with internalized nanoparticles could also adversely influence the screening results. Numerous studies have reported adverse effects of nanoparticles on cell morphology, proliferation, and even DNA integrity (*Pan 2007, Kus 2021*). Therefore, we believe the current setting of Knock-beads is a better solution than the internalized nanoparticles for our screening purpose.

This part of discussion has been included in the revised manuscript "Discussion" section (Page 20, line 488 to line 499).

References:

- Gratton SE*, et al.* The effect of particle design on cellular internalization pathways. *Proc Natl Acad Sci U S A* 2008, **105**(33)**:** 11613-11618.
- Pan Y*, et al.* Size-Dependent Cytotoxicity of Gold Nanoparticles. *Small* 2007, **3**(11)**:** 1941-1949.
- Kus-Liskiewicz M*, et al.* Biocompatibility and Cytotoxicity of Gold Nanoparticles: Recent Advances in Methodologies and Regulations. *Int J Mol Sci* 2021, **22**(20).

6. Line 288, what was used as the negative control, beads without siRNA or with scrambled sequence siRNA?
The negative control is the Knock-beads without loading siRNAs. We have updated the manuscript to clarify this point in "Result" section (Page 13 line 334 to line 335)

7. Line 300, Why the maximum siRNA is 5 not 6? And how come the there were only 54 combinations presented in figure 5f?
As shown in **Figure 5e**, the number of beads interacting with the cells follows a Gaussian-like distribution. In theory, the number of Knock-beads (siRNA loaded) per cell could go beyond 6. The chance of such cases is relatively small given the current bead-to-cell ratio and the spatial constraint of a cell surface. Therefore, we only considered cells with no more than 6 Knock-beads in our first submission to demonstrate the technical capability of this technology.

In fact, in many drug combination therapies, such as the cocktail anti-viral therapy for HIV/AIDS management, 2 to 3 active components are typically used. As shown in **Table R2.1** (*Li 2022*), among more than 20 antiretroviral cocktails, 18 formulations are made of 2 to 3 components and only 2 formulations consist of 4 components. Recently, *Tieu et al*. developed a CRISPR-Cas9-based platform for combinatorial gene editing on CAR-T cells also focused on pairwise combinations (2) of different signaling regulators (*Tieu 2024*) Therefore, we believe that the most informational siRNA cocktail screening should be oriented towards Knock-combos consisting of 2 to 3 siRNAs. With this consideration, we specifically optimized the system and controlled the dose of Knock-beads to ensure ~3 beads per cell on average, as shown in **Figure 5e**. Notably, the number of beads interacting with the cells follows a Gaussian-like distribution, and the center peak of the distribution could be shifted to lower or higher number per cell by controlling the bead-to-cell ratio (**Figure R2.2**). Certainly, the pattern of Knock-bead distribution is crucial for the effectiveness of the combinatorial screening, as it allows for the capture of a diverse range of cell populations that have been randomly exposed to different combinations of siRNAs (Knock-combos). Increasing the bead dose would shift the distribution toward a higher bead number per cell, potentially reducing the population of cells exposed to the desired 2-3 component siRNA cocktails. Conversely, decreasing the bead dose would result in a lower proportion of cells encountering more complex siRNA combinations, which could potentially limit the capability to uncover some effective siRNA combinations. Additionally, over-dosed Knock-beads causes reduced cell viability at the photoporation stage (**Figure R2.3**), which further require an optimization of the bead-to-cell ratio to construct an effective and efficient screening.

Regarding the number of Knock-combo under investigation, for a system involving 6 different Knock-bead variants, theoretically, there are 62 possible combinations. In the practical execution, we were not able to collect data from sufficient occurrence of cells (>20 per replicate) for some Knock-combos (5 or 6 Knock-beads) for statistical analysis, and therefore presented the screening for the observed 54 siRNA combinations. Similar situation was also met in the expanded largescale screening that we conducted in this revision. We further developed an encoding strategy with a 5-channel fluorescent system, which is expanded to encode 31 Knock-bead variants (**Table R2.2**), each of which can be assigned to a specific siRNA. By using this system, we were able to demonstrate an expanded screening involving 20 siRNA targets and tested

more than 1300 Knock-combos composed of 1 to 3 siRNAs for combinatorial anti-tumor gene silencing (**Figure 7**).

This part of discussion has been included in the revised manuscript "Result" section (Page 17, line 411 to Page 19 line 453), and "Discussion" section (Page 21 line 509 to line 523), as well as the supporting information, **Supplementary Note 3** (Page 2, line 56 to line 65).

Table R2.1 List of anti-HIV cocktails and their active components.

Brand name	Ingredients				FDA approve date
Combivir	lamivudine	zidovudine			September 26, 1997
Kaletra	lopinavir	ritonavir			September 15, 2000
Trizivir	abacavir	lamivudine	zidovudine		November 15, 2000
Epzicom	abacavir	lamivudine			August 2, 2004
Triomune	lamivudine	stavudine	nevirapine		not approved
Duovir-N	lamivudine	zidovudine	nevirapine		not approved
Truvada	emtricitabine	tenofovir disoproxil			August 2, 2004
Atripla	emtricitabine	tenofovir disoproxil	efavirenz		July 12, 2006
Complera	emtricitabine	tenofovir disoproxil	rilpivirine		August 10, 2011
Stribild	emtricitabine	tenofovir disoproxil	elvitegravir	cobicistat	August 27, 2012
Triumeq	abacavir	lamivudine	dolutegravir		August 22, 2014
Evotaz	atazanavir	cobicistat			January 29, 2015
Prezcobix	darunavir	cobicistat			January 29, 2015
Dutrebis	lamivudine	raltegravir			February 6, 2015
Genvoya	emtricitabine	tenofovir alafenamide	elvitegravir	cobicistat	November 5, 2015
Odefsey	emtricitabine	tenofovir alafenamide	rilpivirine		March 1, 2016
Descovy	emtricitabine	tenofovir alafenamide			April 4, 2016
Juluca	rilpivirine	dolutegravir			November 21, 2017
Symfi	lamivudine	tenofovir disoproxil	efavirenz		February 5, 2018
Biktarvy	emtricitabine	tenofovir alafenamide	bictegravir		February 7, 2018
Cimduo	lamivudine	tenofovir disoproxil			February 28, 2018
Delstrigo	lamivudine	tenofovir disoproxil	doravirine		August 30, 2018
Dovato	lamivudine	dolutegravir			April 8, 2019
Cabenuva	rilpivirine	cabotegravir			January 21, 2021

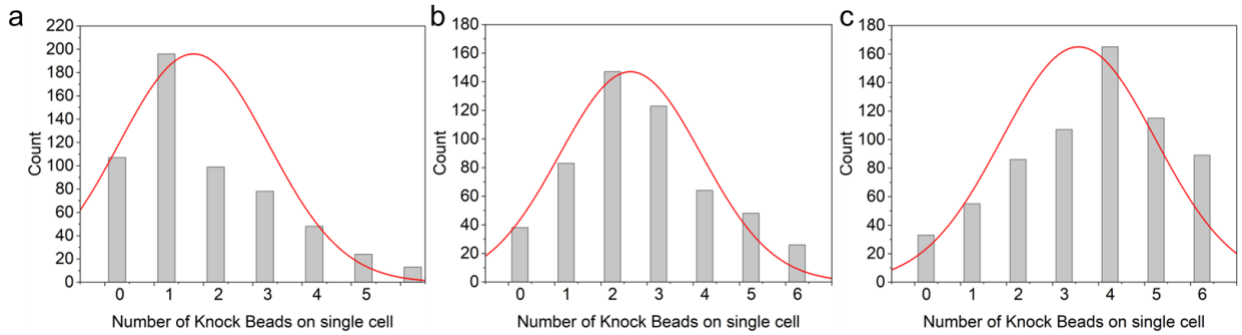

Figure R2.2. Characterization of the Knock-bead distribution per single cell. This figure shows the distribution of the number of Knock-beads per single cell, at different bead-to-cell ratios: 1:1 (a), 2:1 (b), and 4:1 (c). The number of Knock-beads was calculated based on the total number of cells. By controlling the bead-to-cell ratio, we were able to obtain a Gaussian-like distribution of the number of beads interacting with each cell, ranging from 1 to 4 beads per cell. This figure is included in the supporting information as **Supplementary Figure S12**.

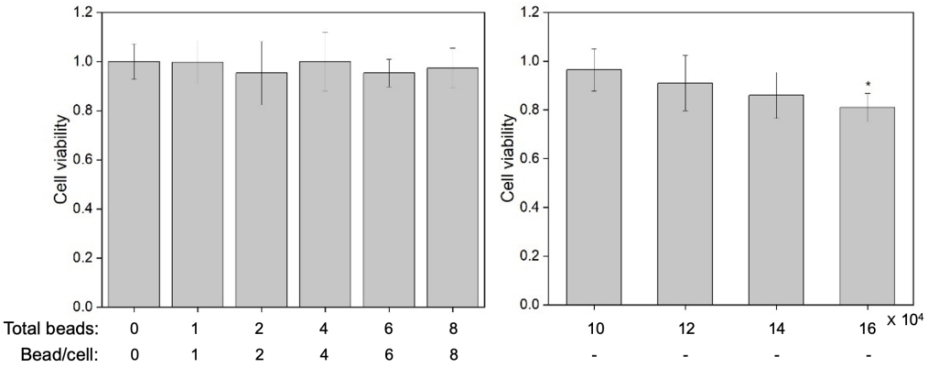

Figure R2.3. Evaluation of cell viability at different Knock-bead to cell ratios. The cell viability was assessed using MTT assay following photoporation treatment at various Knock-bead density. The cells were incubated with Knock-bead at a concentration ranging from 0 to 16 × 10^4. The cell viability was evaluated 24 hours after photoporation. In most screening conditions, the number of Knock-bead per cell would not exceed 8, the photoporation process did not cause any damage in the cells. Only when the Knock-bead density reaches an extremely large level (e.g. 16×10^4), significant cytotoxicity was observed. This figure is included in the supporting information as **Supplementary Figure S13**.

Table R2.2. Spectrum encoding of different Knock-beads using a 5-channel fluorescent system (quantum dot 547, 572, 604, 641, and Alexa fluor 647). The shaded region indicates the extra code not used in the expanded large-scale screening. This table is included in the supporting information as **Supplementary Table S5**.

Knock-bead index	Quantum dot-547	Quantum dot-572	Quantum dot-604	Quantum dot-641	Alexa-647	Code
1	100%	0	0	0	0	10000
2	0	100%	0	0	0	01000
3	0	0	100%	0	0	00100
4	0	0	0	100%	0	00010
5	0	0	0	0	100%	00001
6	100%	100%	0	0	0	11000
7	100%	0	100%	0	0	10100
8	100%	0	0	100%	0	10010
9	100%	0	0	0	100%	10001
10	0	100%	100%	0	0	01100
11	0	100%	0	100%	0	01010
12	0	100%	0	0	100%	01001
13	0	0	100%	100%	0	00110
14	0	0	100%	0	100%	00101
15	0	0	0	100%	100%	00011
16	100%	100%	100%	0	0	11100
17	100%	100%	0	100%	0	11010
18	0	100%	100%	100%	0	01110
19	0	0	100%	100%	100%	00111
20	100%	0	100%	100%	100%	10111
21	100%	100%	100%	100%	100%	11111
22	100%	100%	0	0	100%	11001
23	100%	0	100%	100%	0	10110
24	100%	0	100%	0	100%	10101
25	100%	0	0	100%	100%	10011
26	0	100%	100%	0	100%	01101
27	0	100%	0	100%	100%	01011
28	100%	100%	100%	100%	0	11110
29	100%	100%	100%	0	100%	11101
30	100%	100%	0	100%	100%	11011
31	0	100%	100%	100%	100%	01111

References:
- Li G, *et al.* Approved HIV reverse transcriptase inhibitors in the past decade. *Acta Pharmaceutica Sinica B* 2022, **12**(4)**:** 1567-1590.
- Tieu V, *et al.* A versatile CRISPR-Cas13d platform for multiplexed transcriptomic regulation and metabolic engineering in primary human T cells. *Cell* 2024, **187**(5)**:** 1278-1295 e1220.

8. Should Figure 5e means the number of TYPES of knock beads on a single cell instead of number of knock beads on a single cell as Figure 5f's results were derived from the combination between 6 different types of siRNA/knock bead not total number of siRNA/knock bead on a single cell?

In our first submission, **Figure 5e** was intended to show the distribution of Knock-beads over the cells for optimizing the bead-to-ratio in the screening. The "number" in this panel indicates the exact number of Knock-beads (not bead types) in contact with a cell. In **Figure 5f**, the different Knock-combos indicates the combination of different types of Knock-beads, each of which was loaded with a different siRNA. In an experiment, the Knock-beads of different types (Knock-combos) were applied to the cells with equal concentration (3.6×10^6 beads/mL), therefore, the chances of one cell receives multiple Knock-beads of the same type (Knock-combo) are rare, especially when the screen is targeting more genes (e.g. 20 genes in **Figure 7**). In most cases the number of Knock-beads was equal to the number of types of Knock-beads for a cell. We have clarified relevant information in the revised manuscript "Result" section (Page 14, line 348) and the supporting information as **Supplementary Note 2** (Page 2 line 41 to line 58).

9. What do the black dots in figure 6 a,b,d,e mean? Each dot means one cell? The description of the experimental methods presented in figure 6 in unclear and unfound in materials and method section.

In Figure 6a-e of our first submission, we showed the boxplots with scattered data points to quantify relevant parameters derived from the screening. As pointed out by the reviewer, the black dots indicate the measurements from individual cells, which were collected from 3 independent biological replicates. We have updated the figure caption to include relevant information (Page 40, Figure 6 caption).

Reviewer #3 (Remarks to the Author):

Guo et al. proposed a novel combinatorial siRNA screening method suitable for screening siRNA-based cocktail therapeutics in a massively multiplexed, quantitative, and systematic manner. They utilized assembled nano-/micro composite carriers responsive to near-infrared light and magnetic fields to enable photoporation-induced cellular transfection of RNAs with single-cell resolution. Their innovative approach offers versatile application possibilities. Nonetheless, further validation is necessary to confirm the effectiveness of the proposed new technology.
We thank the reviewer for the positive comments.

1. Given that NIR induces a rise in local temperature around the Knock-beads, it is likely that the heightened concentration of Knock-beads affects cell viability when exposed to NIR, potentially causing thermal damage. Please assess the impact of thermal damage on cell viability in the presence of NIR.
As suggested by the reviewer, we have assessed the impact of thermal damage on cell viability in the presence of NIR. First, we want to point out that NIR irradiation using the selected parameters (980 nm, 16 μs pulse width, 0.6 W/cm^2, 50 Hz) alone does not result in any significant temperature changes (**Figures 3b** and **3c)**. The presence of the Knock-beads leads to localized photothermal effects. As shown in **Figure R3.1**, we evaluated cell viability at different Knock-bead to cell ratios by using MTT assay following photoporation treatment. The cells were incubated with Knock-bead at a concentration ranging from 0 to 16 × 10^4 per culture. The cell viability was evaluated 24 hours after photoporation. In most screening conditions, the number of Knock-bead per cell would not exceed 8, the photoporation process did not cause any apparent damage in the cells, suggesting that the Knock-bead induced temperature change does not harm the cells at these conditions. Only when the Knock-bead density reaches an extremely large level (e.g. 16×10^4 per culture), significant cytotoxicity was observed. For the situation that recapitulate our screening parameters (Knock-bead <= 6 per cell), not much thermal damage was observed in the treated cells. This part of discussion has been added to the manuscript, "Result" section (Page14, line 351 to line 355).

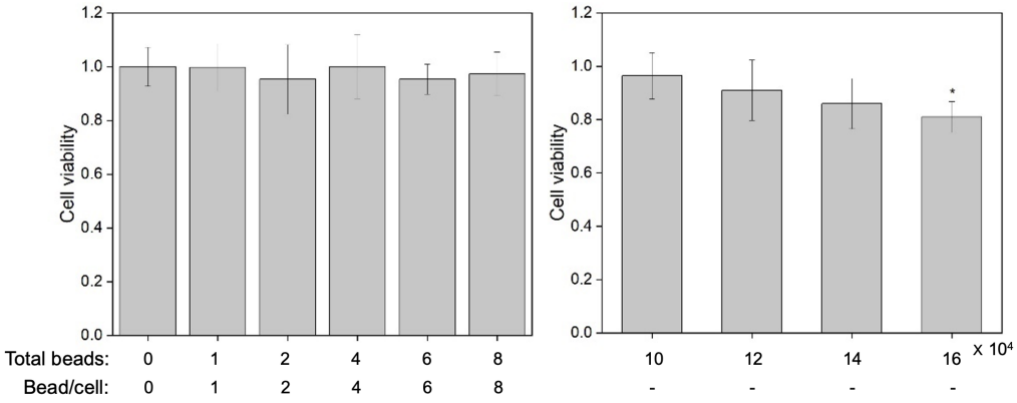

Figure R3.1. Evaluation of cell viability at different Knock-bead to cell ratios. The cell viability was assessed using MTT assay following photoporation treatment at various Knock-bead density. The cells were incubated with Knock-bead at a concentration ranging from 0 to 16 × 10^4 per culture. The cell viability was evaluated 24 hours after photoporation. In most screening conditions, the number of Knock-bead per cell would not exceed 8, the photoporation process did not cause any damage in the cells. Only when the Knock-bead density reaches an extremely large level (e.g. 16× 10^4), significant cytotoxicity was observed. This figure is included in the supporting information as **Supplementary Figure S13**.

2. In Figure 3d, it is evident that as NIR-irradiation times increase, cell viability decreases. Likewise, if there are numerous Knock-beads surrounding the cell, could this influence cell survival rates compared to fewer Knock-beads due to the cytotoxicity of magnetic nanoparticle?
Following our response to point 1 above, we agree with the reviewer that excessive photothermal effects, either by prolonged NIR-irradiation or highly dense application of Knock-bead would compromise cell viability (**Figure R3.1**). For the situation that recapitulate our screening parameters (Knock-bead <= 6 per cell), not much thermal damage was observed in the treated cells.
Additionally, we would like to clarify that: in many drug combination therapies, such as the cocktail anti-viral therapy for HIV/AIDS management, 2 to 3 active components are typically used. As shown in **Table R3.1**(*Li 2022*), among more than 20 antiretroviral cocktails, 18 formulations are made of 2 to 3 components and only 2 formulations consist of 4 components.

Recently, *Tieu et al*. developed a CRISPR-Cas9-based platform for combinatorial gene editing on CAR-T cells also focused on pairwise combinations of different signaling regulators (*Tieu 2024*). Therefore, we believe that the most meaningful siRNA cocktail screening should also be oriented towards Knock-combos consisting of 2 to 3 siRNAs, meaning each cell receives only 2-3 Knock-beads.

This part of discussion has been added to the manuscript "Result" section (Page14, line 351 to line 355) and "Discussion" section (Page 21 line 513 to line 523).

Table R3.1 List of anti-HIV cocktails and their active components.

Brand name	Ingredients				FDA approve date
Combivir	lamivudine	zidovudine			September 26, 1997
Kaletra	lopinavir	ritonavir			September 15, 2000
Trizivir	abacavir	lamivudine	zidovudine		November 15, 2000
Epzicom	abacavir	lamivudine			August 2, 2004
Triomune	lamivudine	stavudine	nevirapine		not approved
Duovir-N	lamivudine	zidovudine	nevirapine		not approved
Truvada	emtricitabine	tenofovir disoproxil			August 2, 2004
Atripla	emtricitabine	tenofovir disoproxil	efavirenz		July 12, 2006
Complera	emtricitabine	tenofovir disoproxil	rilpivirine		August 10, 2011
Stribild	emtricitabine	tenofovir disoproxil	elvitegravir	cobicistat	August 27, 2012
Triumeq	abacavir	lamivudine	dolutegravir		August 22, 2014
Evotaz	atazanavir	cobicistat			January 29, 2015
Prezcobix	darunavir	cobicistat			January 29, 2015
Dutrebis	lamivudine	raltegravir			February 6, 2015
Genvoya	emtricitabine	tenofovir alafenamide	elvitegravir	cobicistat	November 5, 2015
Odefsey	emtricitabine	tenofovir alafenamide	rilpivirine		March 1, 2016
Descovy	emtricitabine	tenofovir alafenamide			April 4, 2016
Juluca	rilpivirine	dolutegravir			November 21, 2017
Symfi	lamivudine	tenofovir disoproxil	efavirenz		February 5, 2018
Biktarvy	emtricitabine	tenofovir alafenamide	bictegravir		February 7, 2018
Cimduo	lamivudine	tenofovir disoproxil			February 28, 2018
Delstrigo	lamivudine	tenofovir disoproxil	doravirine		August 30, 2018
Dovato	lamivudine	dolutegravir			April 8, 2019
Cabenuva	rilpivirine	cabotegravir			January 21, 2021

References:

- Li G, *et al.* Approved HIV reverse transcriptase inhibitors in the past decade. *Acta Pharmaceutica Sinica B* 2022, **12**(4)**:** 1567-1590.
- Tieu V, *et al.* A versatile CRISPR-Cas13d platform for multiplexed transcriptomic regulation and metabolic engineering in primary human T cells. *Cell* 2024, **187**(5)**:** 1278-1295 e1220.

3. Figures 3e-g demonstrate the binding of siRNAs to Knock-beads. Could you provide an estimation of the binding capacity and affinity of Knock-beads for siRNAs? Additionally, is there any impact of siRNA sequence variation on the binding affinity of Knock-beads for siRNAs? Furthermore, when NIR is applied, does it enhance the dissociation of siRNAs from Knock-beads, or does dissociation occur naturally as an on-off effect? Considering the potential dissociation of siRNAs from Knock-beads under culture conditions, there's a possibility of cross-contamination of siRNAs between Knock-beads. Could you elaborate on the likelihood of such cross-contamination?

- Estimation of binding capacity

To provide a quantitative assessment the siRNA loading capabilities of Knock-beads, we have conducted additional experiments and analysis (**Figure 3e**). We used ~8×10^5 Knock-beads to absorb 20 pmol siRNA (cy5 labeled) in the solution through electrostatic interaction. The siRNA loaded Knock-beads were pulled down to the bottom of the reaction tube by an external magnet, depleting the fluorescence in the supernatant solution. We observed that 8 x 10^5 Knock-beads were able to load approximately 64.3% of the 20 pmol of siRNA (9.8×10^6 molecules/bead).

Additionally, in this revision, we evaluated the zeta potential of the beads when loaded with different amounts of siRNA. As shown in **Figure R3.2**, the Knock-beads zeta potential decreased from 22 ± 0.99 mV to 4.71 ± 1.08 mV, as the amount

of loaded siRNA increased from 0 to 80 pmol for a total of 8 x 10^5 beads (equivalent to 0 to 6×10^7 molecules/bead). At even higher siRNA loadings of 160 pmol and 320 pmol (for 8 x 10^5 beads), the zeta potential became negative, measuring -3.33 ± 1.28 mV and -4.4 ± 0.55 mV respectively. When the bead zeta potential is close to "0", it indicates the depletion of the positive charge by the binding of negatively charged siRNAs. Therefore, we estimate that the maximum siRNA loading capacity of 8 x 10^5 Knock-beads is approximately 60 pmol (equivalent to 4.5×10^7 molecules/bead), given the 80 pmol siRNA input and a loading efficiency around 65% (evaluated from **Figure 3e**). This part of discussion has been added to the manuscript (Page 9, line 248 to Page 10 line 253).

- Sequence variation on the binding affinity to Knock-beads

We highly concur the reviewer that it is important for the Knock-beads to perform consistently across different siRNA sequences. To address this concern, we have conducted additional experiment to assess the influence of siRNA sequence variation on the Knock-bead loading efficiency (**Figure R3.3**). In this experiment, we tested the loading efficiency of 8 different siRNA sequences targeting various genes (actin, tubulin, Bcl-2, survivin, Mcl-1, c-Myc, cyclin D1, and PLK1). The results shows that there were no significant differences in siRNA loading on the Knock-beads across these siRNA sequences. This part of discussion has been added to the manuscript "Result" section (Page 10, line 253 to line 254).

- Dissociation of siRNAs from Knock-beads

In this study, the dissociation of siRNAs from Knock-beads is controlled by the NIR irradiation, which is an induced photothermal dynamic process. Regarding the mechanism of siRNA release and cellular entry, we believe that the Poly dimethyl diallyl ammonium chloride (PDDA) layer coating on the surface of the Fe_3O_4-Au beads plays a critical role via van der Waals interactions (*Liu 2015, Kaur 2018, He 2023, Luo 2015*). The PDDA layer was used to electrostatically capture siRNAs. At nanometer scale, the van der Waals adhesion between PDDA and Fe_3O_4-Au bead is increasingly affected by thermal fluctuations (*Carrillo 2012*). Pinon *et al*. demonstrated that a temperature increase of just 23K can lead to a substantial decrease in van der Waals adhesion force from 106 nN to 28 nN (*Pion 2016*). In our system, the temperature of the Knock-beads was changed by gold nanorod-induced surface plasmon resonance (*Amendola 2017, You 2021*). The local temperature increase in each Knock-bead disrupts the van der Waals interactions, causing the PDDA-siRNA detachment from the Knock-beads (**Figure R3.4**). As shown in **Figure R3.4**, we used ~8×10^5 Knock-beads to absorb 20 pmol siRNA-cy5 in the solution through electrostatic interaction. The siRNA loaded Knock-beads were pulled down to the bottom of the reaction tube by an external magnet. Upon NIR irradiation for 2, 4, 6, 8 seconds, the siRNAs were released to the solution by 53.5%, 63.4%, 80.3% and 87.0% of the total load, as reflected by the increase of the fluorescence of the supernatant solution.

This part of discussion has been included in the revised manuscript: "Result" section (Page 10, line 259 to line 266) and "Discussion" section (Page 19, line 473 to Page 20, line 482)

- Likelihood of cross-contamination

As release of siRNA is a triggered process, instead of a naturally happened one, the likelihood of cross-contamination of siRNA in different cells is relatively small. **Figure 4e** provides some important insights into the specificity of siRNA delivery using the Knock-beads. Beyond uncontrolled release of siRNA, the mobility of the Knock-beads from one cell to another could potentially cause diffused error for decoding and analysis. Therefore, it is very important to make sure that the Knock-beads remain fixed on the cells during the analytical process. After application, the Knock-beads were firstly bound to the cell membrane through electrostatic interaction. At the live culture stage, the Knock-beads were further immobilized on the contacting cells using a neodymium magnet (10 kilo-Gauss), which was sufficiently large to prevent the beads from moving around. At the decoding and analysis stage, the cells and the Knock-beads were fixed used polyformaldehyde, where the remaining -NH_2 group on the Knock-beads and cell cytoskeleton was crosslinked. Throughout the processes, the neodymium magnet was kept attached to the bottom of the culture dish to provide sustained restriction of the Knock-beads. The results in **Figure 4a** also showed the specific delivery of the right type of siRNA into individual cells. The knock-beads with either cy5-labeled siRNA (KB1-cy5) or FAM-labeled siRNA (KB2-FAM) were co-cultured with the target cells. For the cells in contact with only KB1-cy5 or KB2-FAM, the majority of the cell population (~90%) showed correct delivery of the designed cargo siRNA-cy5 (carried by KB1-cy5) or siRNA-FAM (carried by KB2-FAM), respectively. These observations indicate that there was minimal cross-contamination from different types of Knock-beads. Again, it is important to note that the Knock-beads are designed with a robust siRNA-loading-release mechanism, and the NIR-triggered release process is well controlled to minimize premature or unintended dissociation of the siRNAs. Together, our Knock-bead system allows the molecular information to be encoded and decoded with reliable linkage to the individual cells.

This part of discussion has been added to the manuscript, “Discussion” section (Page 20, line 488 to line 499).

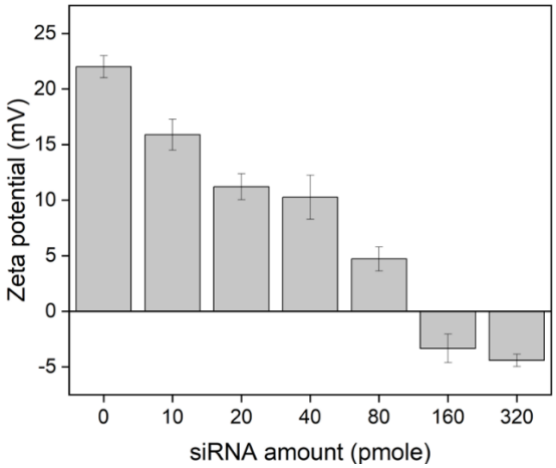

Figure R3.2. Change of Zeta potential for fixed number of Knock-beads (8 x 10^5) with different amount of siRNA loads ranging from 0 pmol to 320 pmol. This figure has been added to the supporting information as **Supplementary Figure S2**.

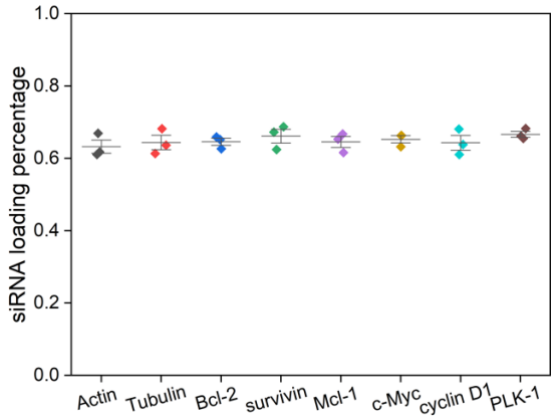

Figure R3.3. Sequence-specific variation of siRNA loading on the Knock-beads. siRNA loading efficiency was tested by measuring the fluorescence depletion (by 8×10^5 Knock-beads) of the supernatant solution originally containing 20 pmol RNAs (cy5-labeled). Cy5-labelled siRNA was absorbed and pulled down by a magnet. Then the fluorescence of the supernatant before and after Knock-bead pulling-down was measured. The loading percentage was calculated by:

$$(Fluorescence_{before} - Fluorescence_{after})/Fluorescence_{before}$$

No significant differences in the loading efficiency across different siRNA sequences, N = 3. This figure has been added to the supporting information as **Supplementary Figure S3**.

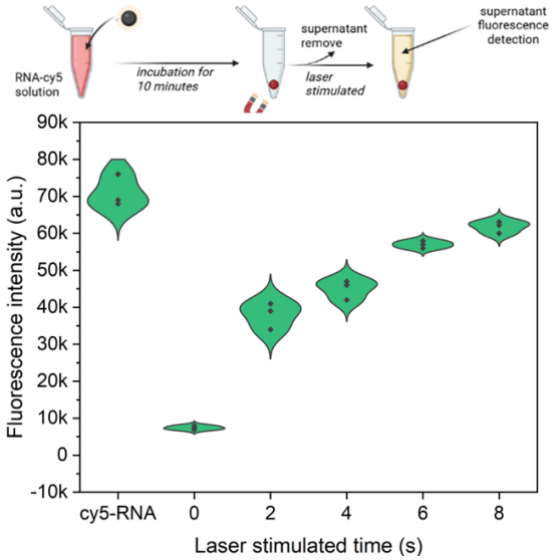

Figure R3.4. Violin plot showing the characterization of siRNA release from the Knock-beads upon NIR irradiation. Fluorescence intensity of the supernatant solution was measured to reflect the RNA capture by the Knock-beads or RNA release from the Knock-beads upon NIR irritation of different duration from 2 to 8 seconds. "0" indicates the depletion of fluorescence by ~8×10^5 Knock-beads to absorb 20 pmol siRNA-cy5 in the solution through electrostatic interaction. The siRNA loaded Knock-beads were pulled down to the bottom of the reaction tube by an external magnet. Upon NIR irradiation for 2, 4, 6, 8 seconds, the siRNAs were released to the solution by 53.5%, 63.4%, 80.3% and 87.0% of the total load, as reflected by the recovery of the fluorescence of the supernatant solution. N = 3, the dots in the violin plots indicate the data points for individual experiments. This figure is included in the revised supporting information as **Supplementary Figure S4**.

References:

- Liu X, *et al.* Understanding the Effect of Different Polymeric Surfactants on Enhancing the Silicon/Reduced Graphene Oxide Anode Performance. *The Journal of Physical Chemistry C* 2015, **119**(11)**:** 5848-5854.
- Kaur P, *et al.* Supramolecular modification of Carbon Nanofibers with Poly(diallyl dimethylammonium) chloride and Triton X-100 for electrochemical application. *International Journal of Hydrogen Energy* 2018, **43**(13)**:** 6575-6585.
- He X, *et al.* Bimodal Antimicrobial Surfaces of Phytic Acid-Prussian Blue Nanoparticles-Cationic Polymer Networks. *Adv Sci (Weinh)* 2023, **10**(16)**:** e2300354.
- Luo D, *et al.* Interparticle Forces Underlying Nanoparticle Self-Assemblies. *Small* 2015, **11**(45)**:** 5984-6008.
- Carrillo J-MY, *et al.* Dynamics of nanoparticle adhesion. *The Journal of Chemical Physics* 2012, **137**(21).
- Pinon AV, *et al.* Thermal effects on van der Waals adhesive forces. *Physical Review B* 2016, **93**(3).
- Amendola V, *et al.* Surface plasmon resonance in gold nanoparticles: a review. *J Phys Condens Matter* 2017, **29**(20)**:** 203002.
- You M, *et al.* Quantifying and Adjusting Plasmon-Driven Nano-Localized Temperature Field around Gold Nanorods for Nucleic Acids Amplification. *Small Methods* 2021, **5**(5)**:** e2001254.

4. This screening must be conducted in the presence of a magnetic field. Prior studies have indicated that exposure to a magnetic field can lead to changes in gene expression, particularly in the expression of heat shock proteins (Bioelectromagnetics. 2014;35(6):406-13, PMID: 24839179). Could you offer insights into how exposure to a magnetic field might affect this screening system?

In the study referenced by the reviewer, the authors explored the effects of pulsed electromagnetic fields (PEMF) on stem cell differentiation and found that a 75 Hz PEMF enhanced the expression of osteogenesis-related markers at early and middle stages. While this study suggests that exposure to PULSED electromagnetic fields can influence gene expression and cellular processes, however, in the context of our study, we used of a STATIC magnetic field to immobilize the Knock-beads, which is a quite different experimental scenario than the referred study. Anyway, everything on earth is always in a static magnetic field. Still, we don't want to rule out the possibility that some specific genes related to magnetic sensing can still be affected, such as bone morphogenetic (BMP) protein belonging to the TGF-β superfamily (*Ongaro A, 2014*). In these cases, extra control group without magnet field should be pre-tested before any actual screening work. This part

of discussion has been added to the manuscript, discussion section (Page20, line 499 to Page 21, line 502).

References:

- Ongaro A, *et al.* Pulsed electromagnetic fields stimulate osteogenic differentiation in human bone marrow and adipose tissue derived mesenchymal stem cells. *Bioelectromagnetics* 2014, **35**(6)**:** 426-436.

5. Figures 4i and j depict the specific knockdown of actin and tubulin by the respective Knock-beads. I think that there may be a mislabeling in the figure legend for Figure 4i. The top-right panel should correspond to KB-A because the Knock-beads are red, while the bottom-left panel should represent KB-T because the Knock-beads are yellow. Moreover, despite the demonstration of the general knockdown effect of each Knock-bead in Figure 4j, it appears that the expression of tubulin is reduced even in the Knock-bead intended for actin (top-right and bottom-left panels in Figure 4i). Could you please clarify the specific knockdown effect of the Knock-beads?

We thank the reviewer for the careful reading of our manuscript. The labeling of **Figure 4** has been properly corrected.

As pointed out by the reviewer, we also observed that silencing actin did influence expression tubulin, which was also previously reported by other groups (*Po'uha 2013*), which have reported crosstalk and interdependence between the actin and tubulin cytoskeletal networks. Disruption or modulation of one component can often impact the expression or organization of the other. Additionally, we have performed quantitative PCR (qPCR) to clarify the siRNA knock down efficacy by direct measurements of the expression level of relevant genes (actin, tubulin, Bcl-2, survivin, Mcl-1, c-Myc, cyclin D1, PLK-1) following the Knock-bead treatment (**Figure R3.5**).

At the protein level, we used western blot to show successful knockdown of actin in A549 cells by using the Knock-beads. For a direct observation with single cell resolution, we also used the Knock-beads to specifically Knock down GFP expression in each individual EGFP-Hela cells that were in contact with the Knock-beads (loaded with siRNA targeting EGFP, labeled with Alexa-647), and the cells showed a significant reduction in EGFP fluorescence (**Figure R3.6**).

This part of discussion has been added to the manuscript, result section (Page 12, line 316 to Page13, line 328)

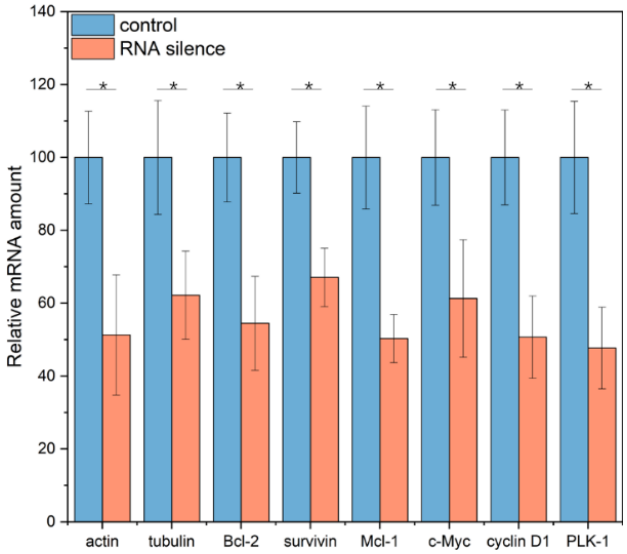

Figure R3.5. Quantitative PCR analysis of knock down efficacy of specific siRNA targeting different genes. Each siRNA was delivered using the Knock-bead mediated photoporation. 24 hours later, the cells were lysed to extract and analyze the mRNA levels by using quantitative real-time PCR. The control group refers to cells that were treated with blank Knock-beads (without any siRNA loaded). The results shows that Knock-bead loaded with specific siRNAs can effectively knock down targeted genes, N=3, $P<0.05$ by student T-test. This figure has been added to the supporting information as **Supplementary Figure S9**.

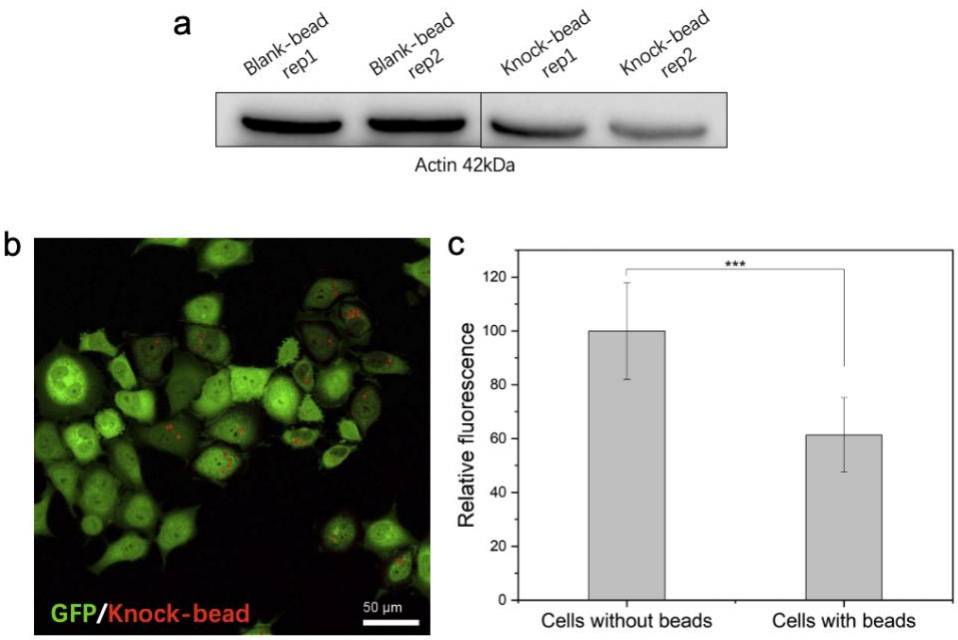

Figure R3.6. Knockdown of protein expression by Knock-bead mediated intracellular delivery of siRNA. (**a**) Western blot result showing successful knockdown of actin expression in A549 cells by using the Knock-beads (loaded with siRNA targeting actin). (**b**) Individual EGFP-Hela cells in contact with the Knock-beads (loaded with siRNA targeting EGFP, labeled with Alexa-647) showed a significant reduction in EGFP fluorescence. (**c**) Quantification of EGFP fluorescence in Hela cells with or without Knock-beads. N = 20, *** indicates P<0.001 by student T-test. This figure has been added to the supporting information as **Supplementary Figure S10**.

References:

- Po'uha ST, *et al.* Partial depletion of gamma-actin suppresses microtubule dynamics. *Cytoskeleton (Hoboken)* 2013, **70**(3)**:** 148-160.

6. In the proof of concept experiments, the knock-down efficiency of 6 siRNA needs to be evaluated for each target gene of siRNAs.

As suggested, we have included additional data to show the knock-down efficiency of the 6 siRNAs, respectively (**Figure R3.5)**. Quantitative PCR (qPCR) analysis directly measures the knockdown efficiency of the various siRNAs-loaded Knock-beads, showing that the Knock-beads loaded with siRNA targeting actin, tubulin, Bcl-2, survivin, Mcl-1, c-Myc, cyclin D1, and PLK-1 all resulted in a significant ($p < 0.05$) reduction in the expression of the respective target genes compared to the control using blank Knock-beads (without siRNA). Relevant discussion has been added to the revised manuscript, "Result" section (Page13, line 319 to Page 14 line 322).

7. When employing color encoding through rainbow labeling, how many genes can be targeted simultaneously using Knock-beads? Please elaborate on this aspect in the discussion section.

As pointed out by the reviewer, the translational potential of a high-throughput technology relies heavily on its extendibility for largescale screens, which appears to be constrained by the availability of fluorophores for simultaneous imaging. The development encoding strategies could overcome this challenge by increasing the screening capacity exponentially. For example, *Shi et al.* have shown that they can use 10 different fluorophores to encode over a thousand (2^{10} - 1) E. coli variants using a machine learning technique (*Shi 2020*). Extended from our work in the first submission, in this revision, we further demonstrated the use of a 5-channel system for multiplexed encoding of more than 30 Knock-beads variants.

Specifically, we used a combinatory fluorescence labeling of the Knock-beads to substantially increase the multiplexing throughput by using 5 fluorescent channels. Each Knock-bead was made with a programmed rainbow fluorescence composed of 5 different fluorophores (quantum dot 547, 572, 604, 641, and Alexa fluor 647). For spectrum digitization, we used "1" to denote the inclusion and "0" to denote the exclusion of a fluorophore and to compose a 5-digit spectral code for each Knock-bead variant. In this way, a 5-channel fluorescent system is expanded to encode 31 Knock-bead variants ($2^5 - 1=31$, **Table R3.2**), each of which was assigned to a specific siRNA. At analytical microscopy stage, the optical spectrum of the Knock-beads was decoded by using a machine learning algorithm (**Figure R3.7**). By using this system,

we were able to demonstrate an expanded screening involving 20 siRNA targets and tested more than 1300 Knock-combos composed of 1 to 3 siRNAs for combinatorial knocking down (**Figure 7**).

Furthermore, an extension to a 10-channel system (*Shi 2020*) with binary labelling ("0" or "1") would increase the multiplexing capacity to over 1023 genes, which would further render millions of Knock-combos. If a screening is designed to target the combinatory silencing of 1023 genes with 2 or 3 siRNA combos, the total possible Knock-combos would be 178,433,024 ($C_{1023}^{2} + C_{1023}^{3}$), which is a number almost inaccessible to any existing methods.

This part of discussion has been added to the manuscript, "Result" section (Page17, line 411 to Page 18, line 434), "Discussion" section (Page21, line 509 to line 523).

Table R3.2. Spectrum encoding of different Knock-beads using a 5-channel fluorescent system (quantum dot 547, 572, 604, 641, and Alexa fluor 647). The shaded region indicates the extra code not used in the expanded large-scale screening. This table is included in the supporting information as **Supplementary Table S5**.

Knock-bead index	Quantum dot-547	Quantum dot-572	Quantum dot-604	Quantum dot-641	Alexa-647	Code
1	100%	0	0	0	0	10000
2	0	100%	0	0	0	01000
3	0	0	100%	0	0	00100
4	0	0	0	100%	0	00010
5	0	0	0	0	100%	00001
6	100%	100%	0	0	0	11000
7	100%	0	100%	0	0	10100
8	100%	0	0	100%	0	10010
9	100%	0	0	0	100%	10001
10	0	100%	100%	0	0	01100
11	0	100%	0	100%	0	01010
12	0	100%	0	0	100%	01001
13	0	0	100%	100%	0	00110
14	0	0	100%	0	100%	00101
15	0	0	0	100%	100%	00011
16	100%	100%	100%	0	0	11100
17	100%	100%	0	100%	0	11010
18	0	100%	100%	100%	0	01110
19	0	0	100%	100%	100%	00111
20	100%	0	100%	100%	100%	10111
21	100%	100%	100%	100%	100%	11111
22	100%	100%	0	0	100%	11001
23	100%	0	100%	100%	0	10110
24	100%	0	100%	0	100%	10101
25	100%	0	0	100%	100%	10011
26	0	100%	100%	0	100%	01101
27	0	100%	0	100%	100%	01011
28	100%	100%	100%	100%	0	11110
29	100%	100%	100%	0	100%	11101
30	100%	100%	0	100%	100%	11011
31	0	100%	100%	100%	100%	01111

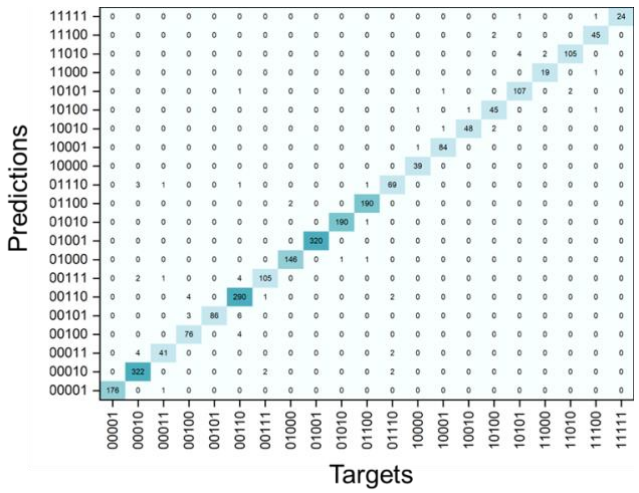

Figure R3.7. Confusion matrix of machine learning-based target prediction for decoding the Knock-beads by using a 5-chanel fluoresce imaging system. The confusion matrix provides an intuitive assessment of the accuracy and performance of the predictive model. The results show that the majority of the targets were predicted correctly, as indicated by the distribution of data points along the diagonal line of the confusion matrix. This suggests a high level of accuracy in the machine learning model's capability to correctly decode different types of Knock-beads. This figure has been added to the supporting information as **Supplementary Figure S16**.

References:

- Shi H*, et al.* Highly multiplexed spatial mapping of microbial communities. *Nature* 2020, **588**(7839)**:** 676-681.

8. In figures 6a and b, apoptosis induction and proliferation inhibition increase with the number of knockdown genes. There is a possibility that this effect is due to non-specific factors such as increased thermal damage resulting from enhanced binding of Knock-beads to cells, rather than specific gene knockdown effects of siRNAs. Please present experimental evidence demonstrating that this effect is not merely a non-specific consequence of an increased number of siRNAs or Knock-beads.

To rule out the possibility of non-specific effects induced by the photo-thermal damage in the cells, we have conducted additional experiments the evaluate the Knock-bead-induced impacts on cell viability (**Figure R3.1)**. First, we want to point out that NIR irradiation of the selected parameters (980 nm, 16 μs pulse width, 0.6 W/cm^2, 50 Hz) alone does not result in significant temperature changes (**Figures 3b** and **3c)**. The presence of the Knock-beads leads to localized photothermal effects. As shown in **Figure R3.1**, we evaluated cell viability at different Knock-bead to cell ratios by using MTT assay following photoporation treatment. The cells were incubated with Knock-bead at a concentration ranging from 0 to 16 × 10^4 per culture. The cell viability was evaluated 24 hours after photoporation. In most screening conditions, the number of Knock-bead per cell would not exceed 8, the photoporation process did not cause any apparent damage in the cells, suggesting that the Knock-bead induced temperature change does not harm the cells at these conditions. Only when the Knock-bead density reaches an extremely large level (e.g. 16×10^4 per culture), significant cytotoxicity was observed. For the situation that recapitulate our screening parameters (Knock-bead <= 6 per cell), not much thermal damage was observed in the treated cells, suggesting the legitimate analysis of apoptosis induction and proliferation inhibition regulated by with the combinatorial knockdown targeted genes by using the Knock-bead system. This part of discussion has been added to the manuscript, “Result” section (Page14, line 351 to line 355).

9. In figures 6d and e, the effects of single-path-2 or single-path-3 may vary depending on the targeted pathways (apoptosis or proliferation). Please compare the effects of single-path-2 or single-path-3 from the apoptosis pathway, proliferation pathway, and their combination on the apoptosis and proliferation.

As suggested, we compared the anti-tumor efficacy of single pathway knock-down or dual pathway know-down targeting either apoptosis (single-path-apo)/proliferation (single-path-pro) or the combination of the two pathways (dual-path). This comparison included knock-combos involving all 2 and 3 siRNAs (**Figure R3.8)**. The results generally show that siRNAs targeting multiple pathways give better anti-tumor efficacy. Similar conclusion can also be drawn from our expanded largescale screen involving 20 siRNA targets with more than 1300 Knock-combos composed of 1 to 3 siRNAs for combinatorial anti-tumor gene silencing (**Figure 7c**). This part of discussion has been added to the manuscript, “Result” section (page 16, line 385 to line 387).

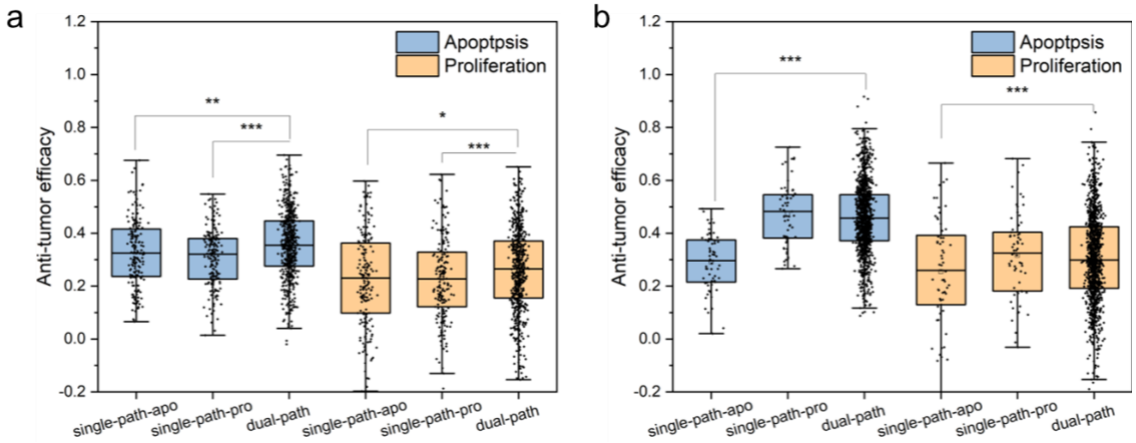

Figure R3.8. Analysis of combinatorial knock down by siRNAs targeting multiple signal pathways by using (**a**) Two siRNA Knock-combos, (**b**) Three siRNA Knock-combos. "Single-path-apo" refers to combinations containing siRNAs exclusively targeting the apoptosis pathway. "Single-path-pro" refers to combinations containing siRNAs exclusively targeting the proliferation pathway. "Dual path" refers to combinations containing siRNAs targeting both the apoptosis and proliferation pathways. * P< 0.05, ** P<0.01, *** P< 0.001 by Wilcoxon rank sum test. This figure has been added to the supporting information as **Supplementary Figure S14**.

10. In the discussion, the authors propose the possibility of expanding the siRNA screening throughput to encompass more than 60 genes. It would be valuable to provide experimental evidence showing that this approach can be implemented at the single-cell level using an increased number of Knock-beads. It is suggested that the distribution of the number of Knock-beads on individual cells, as illustrated in Figure 5e, should be demonstrated for at least 20 types of Knock-beads. Additionally, could there be resolution issues when observing a large number of beads, each with different labels, under a microscope? Please elaborate on the resolution issues encountered when using a large number of Knock-beads.

We thank the reviewer for the helpful suggestions and concur the reviewer that the translational potential of a high-throughput technology relies heavily on its extendibility for largescale screens. Towards this goal, we want to firstly clarify the concept of combinatorial screening before constructing a larger scale screening involving more siRNA gene targets. In many drug combination therapies, such as the cocktail anti-viral therapy for HIV/AIDS management, 2 to 3 active components are typically used. As shown in **Table R3.1** (*Li 2022*), among more than 20 antiretroviral cocktails, 18 formulations are made of 2 to 3 components and only 2 formulations consist of 4 components. Recently, *Tieu et al.* developed a CRISPR-Cas9-based platform for combinatorial gene editing on CAR-T cells also focused on pairwise combinations of different signaling regulators (*Tieu 2024*). Therefore, we believe that the most meaningful siRNA cocktail screening should also be oriented towards Knock-combos consisting of 2 to 3 siRNAs. With this consideration, it is worth noticing that even more siRNAs for different gene targets are screened (e.g. 20 gene targets in our extended demonstration), the on-average number of Knock-beads per individual cells should be tuned to be 2~3 to evaluate their combinatorial efficacy, which would NOT be a significant burden for microscopy to resolve the beads on the single cell level. More importantly, the challenging part would be the phenotypic extraction of the large number of Knock-combos in the overall cell population, which would require innovation in the following two aspects: 1) multiplexed encoding siRNA-loaded Knock-beads; 2) Phenotypic analysis and decoding of Knock-combos in large number of cells.

For multiplexed encoding, we used a combinatory fluorescence labeling of the Knock-beads to substantially increase the multiplexing throughput by using 5 fluorescent channels. Each Knock-bead was made with a programmed rainbow fluorescence composed of 5 different fluorophores (quantum dot 547, 572, 604, 641, and Alexa fluor 647). For spectrum digitization, we used "1" to denote the inclusion and "0" to denote the exclusion of a fluorophore and to compose a 5-digit spectral code for each Knock-bead variant. In this way, a 5-channel fluorescent system is expanded to encode 31 Knock-bead variants ($2^5 - 1=31$, **Table R3.2, Figure R3.7**, **Figure R3.9**), each of which can be assigned to a specific siRNA. At analytical microscopy stage, the optical spectrum of the Knock-beads was decoded by using a machine learning algorithm to analyze the fluorescence spectrum (**Table R3.3**) (*Breiman 2001*). Furthermore, an extension to a 10-channel system with binary labelling ("0" or "1") would increase the multiplexing capacity to over 1023 genes, which would further render millions of Knock-combos. If a screening is designed to target the combinatory silencing of (*Shi 2020*) 1023 genes with 2 or 3 siRNA combos, the total possible Knock-combos would be 178,433,024 ($C_{1023}^2 + C_{1023}^3$), which is a number almost inaccessible to any existing methods.

This part of discussion has been added to the manuscript, “Result” section (Page 17, line 411 to Page19 line 453), “Discussion” section (page 21, line 509 to line 523)

In the practical large scale siRNA screening targeting the 20 genes spreading over 6 different cellular pathways: membrane interaction (5 siRNAs), apoptosis (4 siRNAs), cell cycle (2 siRNAs), DNA repair (3 siRNAs), drug resistance (1 siRNA), and oncogenesis (5 siRNAs). The phenotypic induction of cellular apoptosis was analyzed for more than 1300 Knock combos involving 1, 2 or 3 siRNAs targeting a subset of the 20 genes. The screening results were summarized in the newly included **Figure 7**,

While the apoptosis level varied among different Knock-combos, it was clearly observed multi-pathway knock-down was more effective than just targeting a single-pathway. Such synergic efficacy becomes even more evident for 3 siRNA combinations (**Figure 7c**), which is consistent with our observations in the smaller scale screening and emphasizes the importance and unique advantage of our innovation for high-throughput combinatorial siRNA screening. For all the 1315 siRNA Knock-combos, K-means clustering analysis was used to discover two distinct clusters, one of which showed significantly better efficacy for apoptosis induction (**Figure 7d, e, Supplementary Figure S17**). We then derived a relative ratio to show the enrichment of individual siRNA in each cluster (cluster 1, 2), showing the top-6 dominant role of cyclin D1, survivin, HER-2, Hsp 27, Upar and GSK 3a for the apoptosis-pro cluster (cluster 1, **Figure 7f**), which are well-represented in the top-2 apoptosis-pro Knock-combos (**Figure S18**). We then used a network interaction diagram to analyze the synergic efficacy from multiple siRNAs (**Figure 7g**). As a hub gene, HER2 or cyclin D1 showed the most connections to other genes, suggesting the important contributions from siRNAs targeting complementary genes. On the other hand, uPAR gene appeared to be the best silencing partner for many leading siRNA targeting either survivin or HER2. These screening results provides valuable insights to the construction of combinatorial siRNAs therapeutics for anti-tumor purpose.

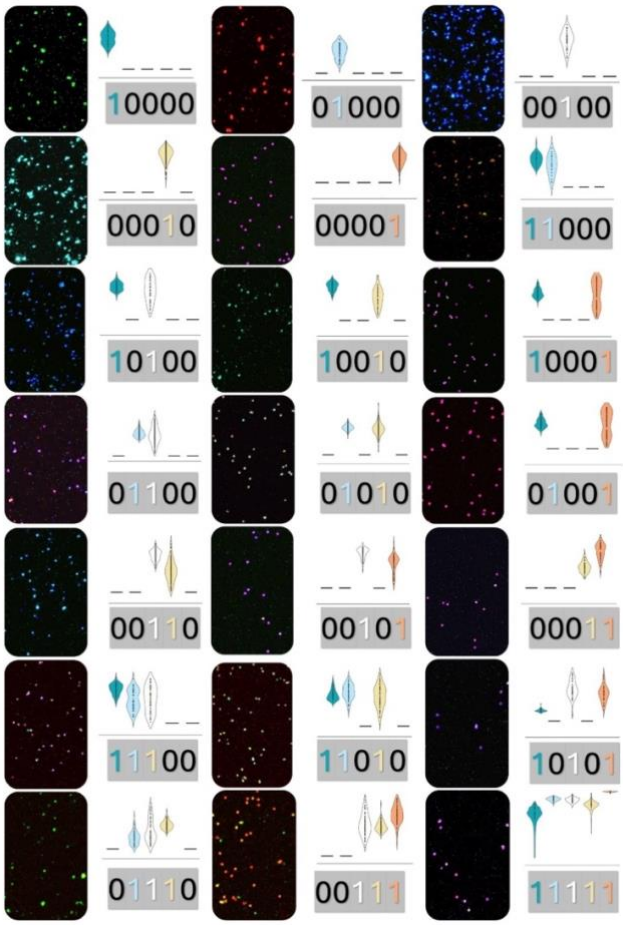

Figure R3.9. Representative images showing the encoded fluorescence signal of 21 Knock-bead variants. A combinatory fluorescence labeling of the Knock-beads was used to substantially increase the multiplexing throughput by using 5 fluorescent channels. Each Knock-bead was made with a programmed rainbow fluorescence composed of 5 different fluorophores (quantum dot 547, 572, 604, 641, and Alexa fluor 647). For spectrum digitization, we used "1" to denote the inclusion and "0" to denote the exclusion of a fluorophore and to compose a 5-digit spectral code for each Knock-bead variant. This figure is included in the supporting information as **Supplementary Figure S15**.

Tale R3.3. Knock-bead decoding performance for a 5-channel encoding system. This table has been added to the supporting information as **Supplementary Table S6**.

Statistics	Results
Accuracy	0.9748
95% CI	(0.9595,0.9856)
P-value	<0.0001
Kappa	0.9728
Multiclass area under the curve	0.9982

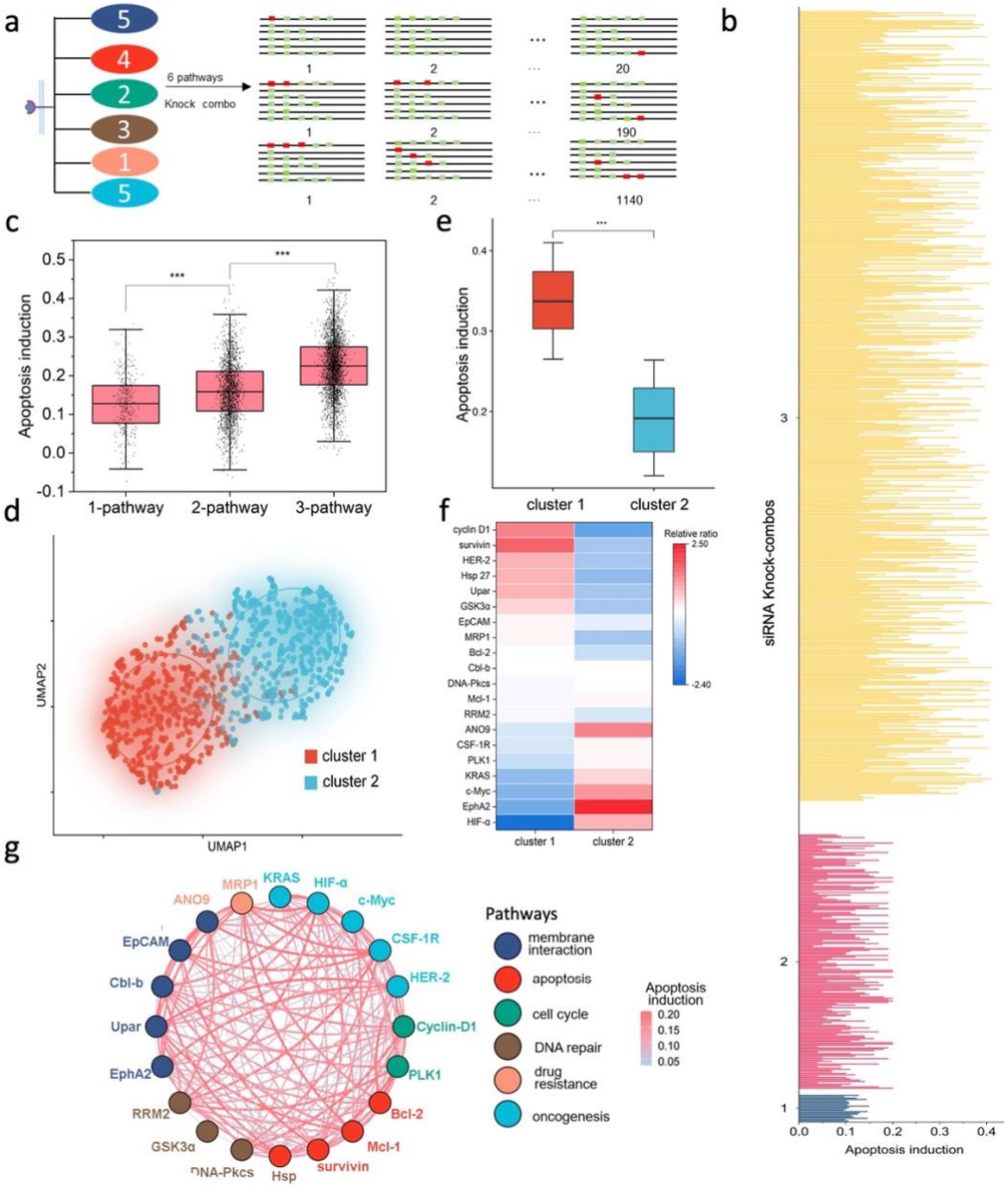

Figure 7. Expanded screening of 1315 Knock-combos composed of 1, 2, or 3 siRNAs targeting 20 genes. (**a**) A set of 20 siRNAs targeting 6 different cellular pathways: membrane interaction (5 siRNAs), apoptosis (4 siRNAs), cell cycle (2 siRNAs), DNA repair (3 siRNAs), drug resistance (1 siRNA), and oncogenesis (5 siRNAs). The screening space (1350) is composed of 20 1-siRNA, 190 2-siRNA and 1140 3-siRNA Knock-combos. (**b**) Phenotypic analysis of apoptosis induction for all the tested 1-siRNA (blue), 2-siRNA (red) and 3-siRNA (yellow) Knock-combos. Data were collected from more than 20 cells for each of the 1315 Knock-combos. (**c**) Boxplots with scattered data points showing the comparison of the efficacy on apoptosis induction for combinatorial targeting of single, dual or multiple signaling pathways. (**d**) K-means clustering analysis of all the Knock-combos reveals two distinct clusters in the UMAP space. (**e**) Boxplots showing the comparison of apoptosis induction for the 2 identified Knock-combo clusters. (**f**) Enrichment analysis of the 20 siRNA targets in each identified Knock-combo clusters. (**g**) An interaction network showing the synergic co-operation in apoptosis induction for the 20 siRNAs to different gene targets, where the line color and thickness indicate the phenotypic efficacy of the corresponding combination. * P< 0.05, ** P<0.01, *** P< 0.001 by T test.

References:

- Li G, *et al.* Approved HIV reverse transcriptase inhibitors in the past decade. *Acta Pharmaceutica Sinica B* 2022,

12(4)**:** 1567-1590.
- Tieu V*, et al.* A versatile CRISPR-Cas13d platform for multiplexed transcriptomic regulation and metabolic engineering in primary human T cells. *Cell* 2024, **187**(5)**:** 1278-1295 e1220.
- Shi H*, et al.* Highly multiplexed spatial mapping of microbial communities. *Nature* 2020, **588**(7839)**:** 676-681.
- Breiman L. Random Forests. *Machine Learning* 2001, **45**(1)**:** 5-32.

11. As stated in the method (Lines 507–508), the TUNEL Apoptosis Assay was conducted after 20 hours of photoporations. This timeframe could be beneficial for identifying genes associated with short-term cell death. However, if employing combinatorial siRNA screening to unveil genes involved in long-term cell death, it's pertinent to consider whether spectrum-coded Knock-beads can sustain the stability of fluorophores and, if so, for how long.

We agree with the reviewer that the long-term fluorescence stability would affect the usage of spectrum-coded Knock-beads for screening of long-term cellular function and relevant phenotypes. Therefore, in this revision, we conducted a 7-day experiment to test the photo-stability of the fluorophore-modified Knock-beads (quantum dot 547, 572, 604, 641, and Alexa fluor 647) in DMEM cell culture medium. Every 24 hours, the Knock-beads were magnetically isolated to access their fluorescence intensity by using a microplate reader. Over the 7-day incubation period, the fluorescence was sustained without much bleaching (**Figure R3.10**) and should be applicable to analyze cellular function and relevant phenotypes over a longer temporal window beyond 20 hours.

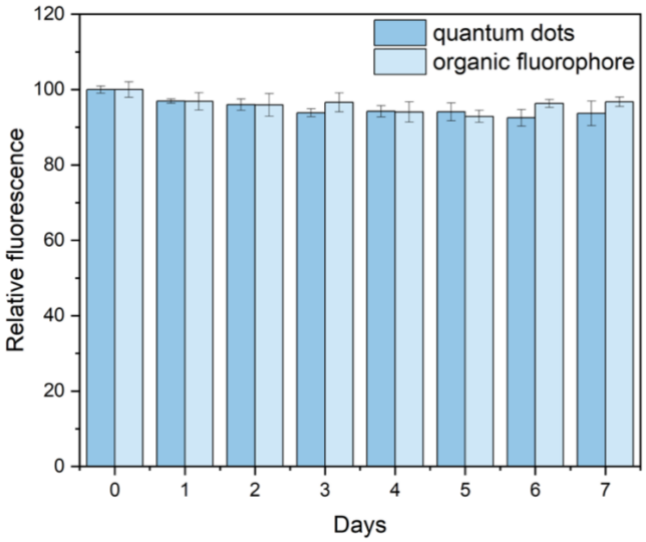

Figure R3.11. Analysis of fluorescence stability of the labeled Knock-beads in cell culture medium over a 7-day incubation period. The Knock-beads were rainbow labeled by quantum dot 547, 572, 604, 641, and Alexa fluor 647, and then incubated with DMEM medium at 37°C. Every 24 hours, the Knock-beads were magnetically separated from the medium, and their fluorescence was measured using a plate reader. The results show the temporal photostability for potential long-term screening.